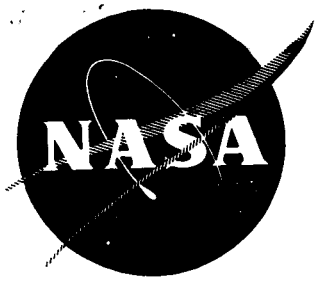

FUEL CELL RESEARCH

AN INVESTIGATION OF NON-STEADY-STATE OPERATION

by

T. J. Gray, A. A. Schneider, R. B. Rozelle

prepared for

NATIONAL AERONAUTICS AND SPACE ADMINISTRATION

GRANT NsG-384

Alfred University
Alfred, New York

NOTICE

This report was prepared as an account of Government sponsored work. Neither the United States, nor the National Aeronautics and Space Administration (NASA), nor any person acting on behalf of NASA:

A.) Makes any warranty or representation, expressed or implied, with respect to the accuracy, completeness, or usefulness of the information contained in this report, or that the use of any information, apparatus, method, or process disclosed in this report may not infringe privately owned rights; or

B.) Assumes any liabilities with respect to the use of, or for damages resulting from the use of any information, apparatus, method, or process disclosed in this report.

As used above, "person acting on behalf of NASA" includes any employee or contractor of NASA, or employee of such contractor, to the extent that such employee or contractor of NASA, or employee of such contractor prepares, disseminates, or provides access to, any information pursuant to his employment or contract with NASA, or his employment with such contractor.

Requests for copies of this report should be referred to

National Aeronautics and Space Administration
Office of Scientific and Technical Information
Attention: AFSS-A
Washington, D. C. 20546

THIRD SEMIANNUAL REPORT

FUEL CELL RESEARCH

An Investigation of Non-Steady-State Operation

by

T. J. Gray, A. A. Schneider, R. B. Rozelle

prepared for

NATIONAL AERONAUTICS AND SPACE ADMINISTRATION

Period: June 1 - December 31, 1964

Contract NsG-384

Technical Management
NASA Lewis Research Center
Cleveland, Ohio
Solar and Chemical Power Branch
William J. Nagle

ALFRED UNIVERSITY
Alfred, New York

TABLE OF CONTENTS

INTRODUCTION

In this, the third semiannual report on the investigation of non-steady-state operation of fuel cells, further information is presented on the improvement in the operating capability of the hydrogen-oxygen fuel cell resulting from pulsed load operation. Moderate improvements of power output (10 to 15%) have been realized with existing equipment and it is believed that greater improvement can be achieved under heavier pulse loading conditions for which equipment has recently been completed but not yet tested. In order to assess feasibility of application of this technique to power generating systems, the new test equipment has been developed as a three-phase unit capable of deriving fundamental and applicational data simultaneously.

Whereas the feasibility of realizing improved performance has been demonstrated and can now be studied in greater detail with the poly-phase interrupter loading unit, nevertheless it is now abundantly clear that for a fuller understanding of the individual electrode reactions, it will be necessary simultaneously to study simplified single electrodes under corresponding pulsed operation conditions. In a separate study, it has been demonstrated that galvanostatic techniques can provide valuable information regarding the constitution of the catalyst under specific operating conditions and an extension of this study to simulate more closely fuel cell operating conditions will be undertaken in the near future. Measurements of a fundamental nature have been conducted on palladium-gold and platinum-palladium alloys in order to establish the fundamental validity of interpretations derived from the galvanostatic technique and to provide the necessary background for an appraisal of catalyzed fuel cell electrodes. This work is to be submitted for publication to the Royal Society, London, in the immediate future.

Whereas the corresponding research by Union Carbide Corporation (NASA Contract NAS3-6460) has demonstrated that a significant improvement to fuel cell operation can be achieved by heavy intermittent pulsing of a fuel cell apparently resulting from catalyst activation, the present investigation suggests that an additional or comparable improvement can be realized by continuously interrupting the load on the cell. It cannot, at this juncture, be ascertained whether both effects would be observed simultaneously.

PART I

AN INVESTIGATION OF A PULSE LOADED HYDROGEN-OXYGEN FUEL CELL

The discharge characteristics of a hydrogen-oxygen fuel cell have been investigated in detail employing the technique of pulse loading. Power output of the cell under these conditions has been studied from the standpoint of duty time of the pulse, frequency of the pulse and per cent duty cycle of loading at a wide range of polarizing current densities. Although individual electrode behavior under "pulse loading" conditions has not been studied to this time, the data demonstrate that improvements of the power output of the fuel cell up to 15% can be realized from pulse loading. Optimum conditions within the range of the pulse generator are given and discussed. The effect of the above parameters on concentration polarization and internal resistance of the cell is also discussed.

EXPERIMENTAL PROCEDURE

The hydrogen-oxygen fuel cell studied had a 30% potassium hydroxide electrolyte held in an asbestos matrix. Electrode material (Clevite No. 3) was obtained from the Clevite Corporation and consisted of a nickel wire mesh covered with porous sintered nickel. The electrode material which was to serve as the hydrogen electrode was subjected to ultrasonic agitation in a 2% platinum-2% palladium chloride solution; this same solution was then used to electrolytically co-deposit the platinum-palladium black as the catalytic agent. A similar procedure was employed for the oxygen electrode using a 4% platinum chloride solution. The apparent area of each electrode was 1.76 cm^2. Hydrogen and oxygen pressures employed during operation were 3.0 cm Hg, and the temperature of the cell was maintained constant at 60° C.

The external circuit consisted of a pulse generator and current set resistors shown in the pulse loading circuit (Figure 1). These were adjusted to give a specific pulse duration, frequency, and average current. The cell was subjected to a steady loading at a current which was the same as that set in the pulse loading circuit. When equilibrium was established under steady loading, the potential was recorded and the cell was quickly switched to pulse loading circuit. The average potential under pulsed loading at this set pulse duration and frequency was then recorded. With the average current held constant, the average potentials at different pulse durations and frequencies were also recorded. This procedure was repeated for many average currents to give discharge curves for the cell under conditions of steady and pulsed loading.

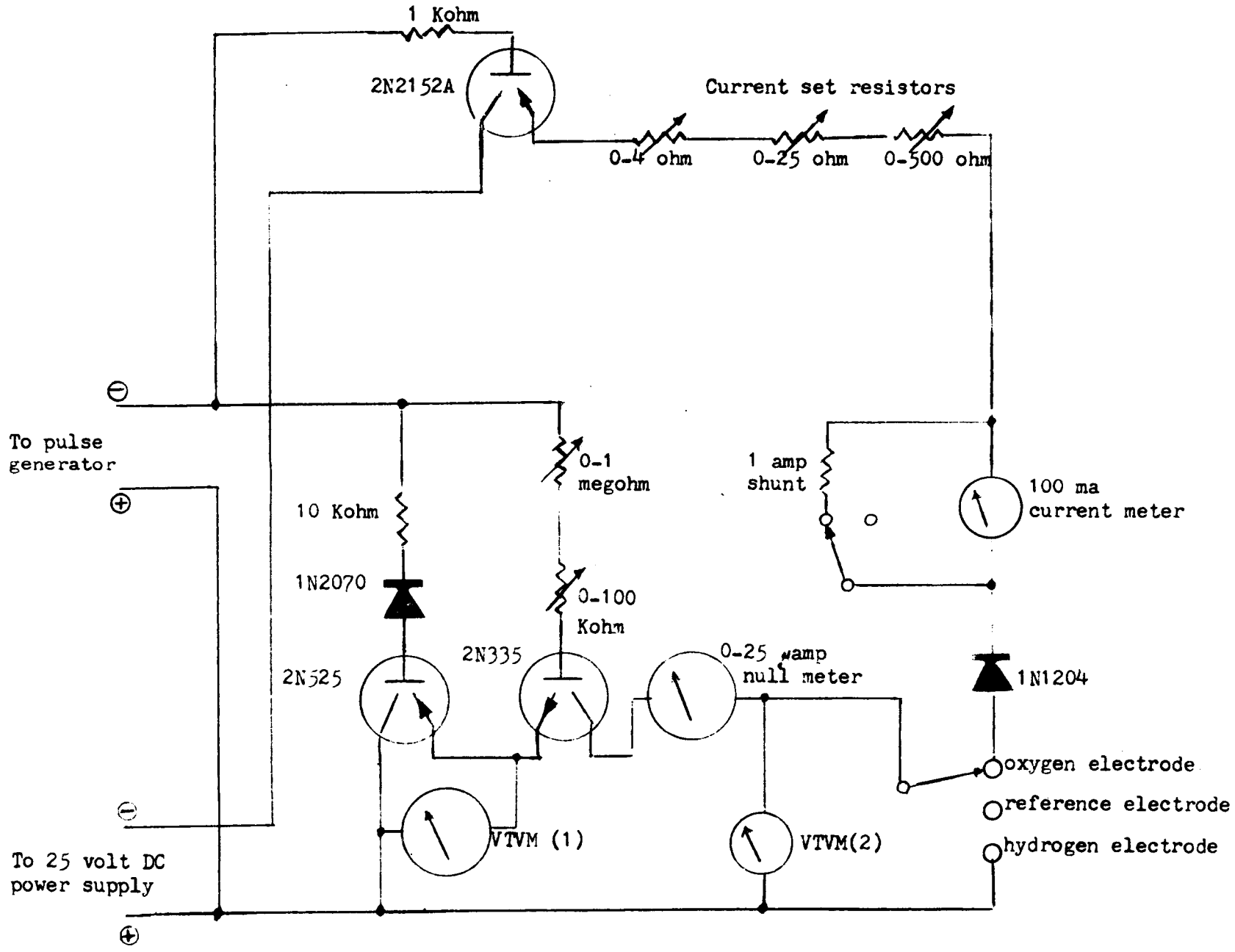

FIGURE 1. Pulse Loading Circuit

The potentials recorded at high currents were not obtained under equilibrium conditions, but rather while the cell was very slowly decaying. These points, however, were obtained in a time interval which was short enough to make the decay insignificant.

The same cell was investigated using 30% potassium hydroxide electrolyte without the asbestos matrix. The performance of this cell under steady load was considerably better than the cell using the asbestos matrix, but a comparison of the improvement in performance under pulsed loading showed that the cell with the asbestos matrix gave a larger power increase at potentials below 1 volt than did the cell with the liquid electrolyte.

Because of physical limitations, it was difficult to incorporate a reference electrode in the fuel cell. This difficulty is now being corrected and data on the individual fuel electrodes will be included in the next report.

RESULTS

Numerous runs were made to study the effects of various parameters involved in pulse loading on the discharge curves of a hydrogen-oxygen fuel cell. A composite data sheet of these runs is given in Table I. It is emphasized that these data are typical of results obtained and are reproducible.

All fuel cell voltages shown in Table I and represented henceforth in graphs are terminal voltages and are considered average voltages under pulsed load. Similarly the current densities represent averages under pulsed load.

Duty time represents the length of time a load is across the cell for one cycle. The frequency of the pulse is also shown. The per cent duty cycle is:

$$\text{Duty time} \times \text{frequency} \times 100 = \%\ \text{duty cycle},$$

and gives the per cent time which the cell is loaded. For instance, the first duty time given for pulsing is 20×10^{-6} seconds, and at a signal frequency of 2000 cycles/second, the per cent duty cycle is 4%.

An average current density (c.d.) is obtained in a usual manner with a 100% duty cycle, i.e., with an external power supply providing the polarizing current equal to the average c.d. Under pulsed load, however, the polarizing current must be much higher to provide the same average current density as with 100% duty cycle since the load is on only a small fraction of the time. For example, a polarizing current density of 1000 ma/cm^2 at 1% duty cycle must be used to produce an average current density load of 10 ma/cm^2 on the cell. Hence, a

Table I

Composite Data Sheet

Duty Time (microseconds)	Current Density (ma/cm^2)	Steady Load	Fuel Cell Voltage (volts) 2000 cyc/sec	1000 cyc/sec	500 cyc/sec
		100% duty cycle	4% duty cycle	2% duty cycle	1% duty cycle
20	0	1.23	1.23	1.23	1.23
	5.7	1.08	1.08	1.10	1.12
	11.4	0.99	1.00	1.02	1.04
	17.1	0.83	0.88	0.93	0.95
	22.8	0.48	0.52	0.54	0.55
	28.5	0.10	0.15	0.17	0.17
		100% duty cycle	8% duty cycle	4% duty cycle	2% duty cycle
40	0	1.23	1.23	1.23	1.23
	5.7	1.08	1.08	1.09	1.10
	11.4	0.99	0.99	0.99	1.01
	17.1	0.83	0.86	0.88	0.93
	22.8	0.48	0.51	0.52	0.54
	28.5	0.10	0.13	0.15	0.17
		100% duty cycle	16% duty cycle	8% duty cycle	4% duty cycle
80	0	1.23	1.23	1.23	1.23
	5.7	1.08	1.08	1.08	1.08
	11.4	0.99	0.99	0.99	1.00
	17.1	0.83	0.84	0.86	0.89
	22.8	0.48	0.49	0.51	0.52
	28.5	0.10	0.11	0.12	0.14

limiting factor in the experiments, thus far, has been the maximum current which can be pulsed through the circuit. This maximum current is determined by the maximum allowable voltage of the external power supply and the resistance of the pulse loading circuit.

Figure 2 is illustrative of the variation of the discharge curve of the fuel cell at 60°C as a function of current loading at various frequencies. Duty time of the pulse is 20 microseconds. Improvement in the discharge curve is most pronounced at the lowest frequency (500 cycles/second) and 1% duty cycle as is indicated graphically in Figure 3. The improvement decreases as the frequency increases; that is, as the per cent duty cycle increases. The effect becomes more apparent as the load on the cell increases up to ca 18 ma/cm^2 where the cell polarizes rapidly. As indicated previously, the data beyond this point are quasi-steady state and its value is difficult to assess. The limiting current density for the cell appears to be of the order of 20 ma/cm^2. It is in the region where the cell begins to polarize rapidly that the greatest improvement in the cell potential is realized from pulse loading.

The limiting current density, I_L, which is established in the fuel cell may be due to either gas or electrolyte concentration polarization at either electrode. Since the 30% potassium hydroxide electrolyte is held in an asbestos matrix which would most likely impede the transport of ions, it will be assumed that I_L is due to an electrolyte concentration effect. In that two separate electrochemical reactions are occurring within the cell and since no reference electrode was employed, it is not possible to determine which reaction is limited by the concentration polarization. For the sake of discussion, however, it will be assumed that the hydrogen electrode is polarized due to the electrolyte concentration gradient and that the oxygen electrode polarization, due to a concentration gradient, is negligible. With equal justification, it could be assumed that the oxygen electrode is polarized due to a buildup in concentration of peroxide ion at the oxygen electrode. The polarization of the cell, then, might be a result of either one of these conditions separately or a result of the simultaneous existence of both. Since, however, mathematical treatment of this latter condition is not as well defined, for the sake of simplicity, a treatment of concentration polarization at the hydrogen electrode will be given.

Because of the difficulty involved in determining which of the electrodes is primarily responsible for polarization of the cell, it is obvious that a study of each individual fuel electrode would be of great value. Perhaps even more information could be gained from a study of an electrode which is more reproducible than the fuel electrode; for example, the Ag/Ag^+ electrode. With an electrode such as this, the various factors affecting polarization could be more easily controlled and studied under pulsed loading.

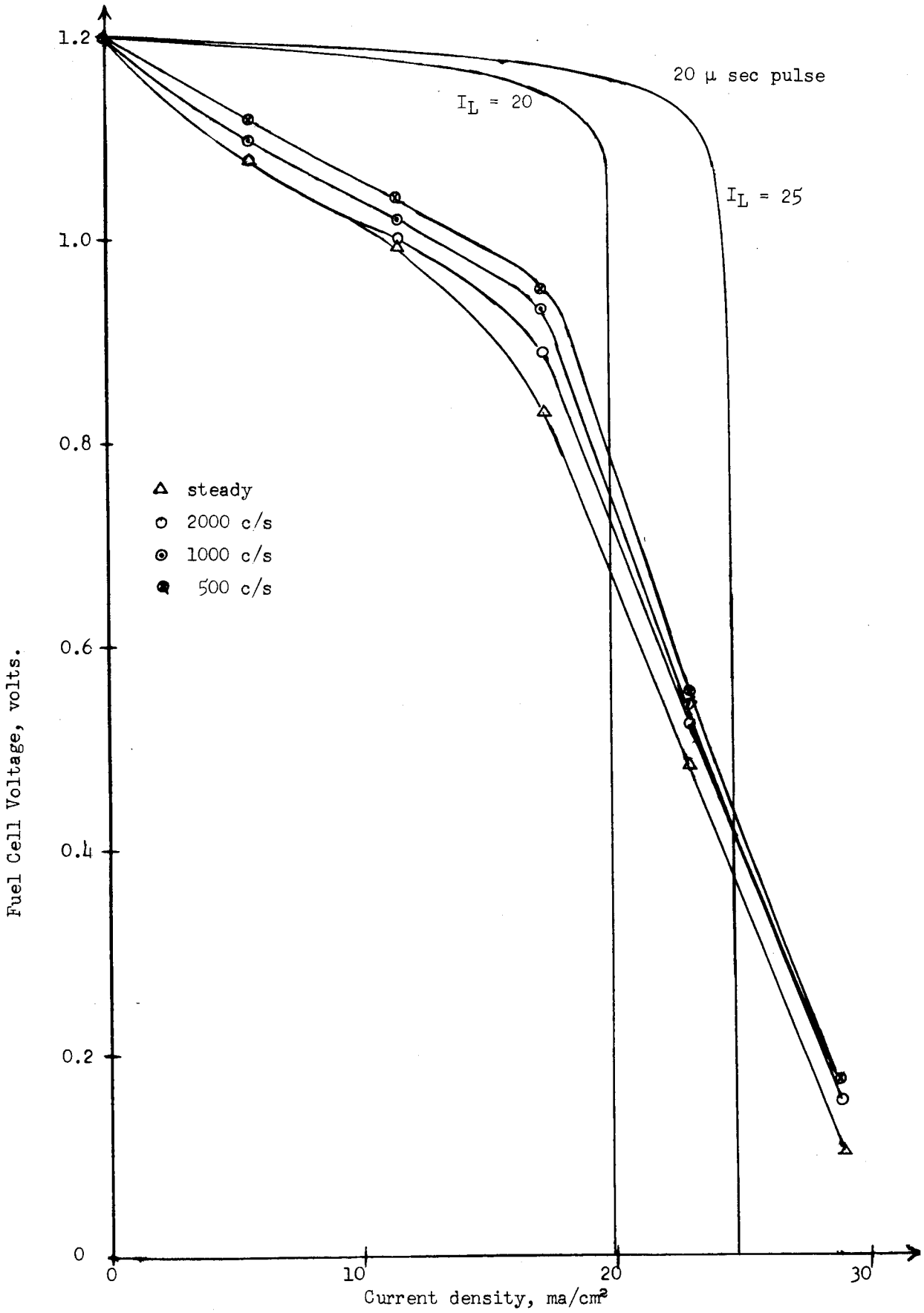

Figure 2. Comparison of Experimental and Calculated Data.

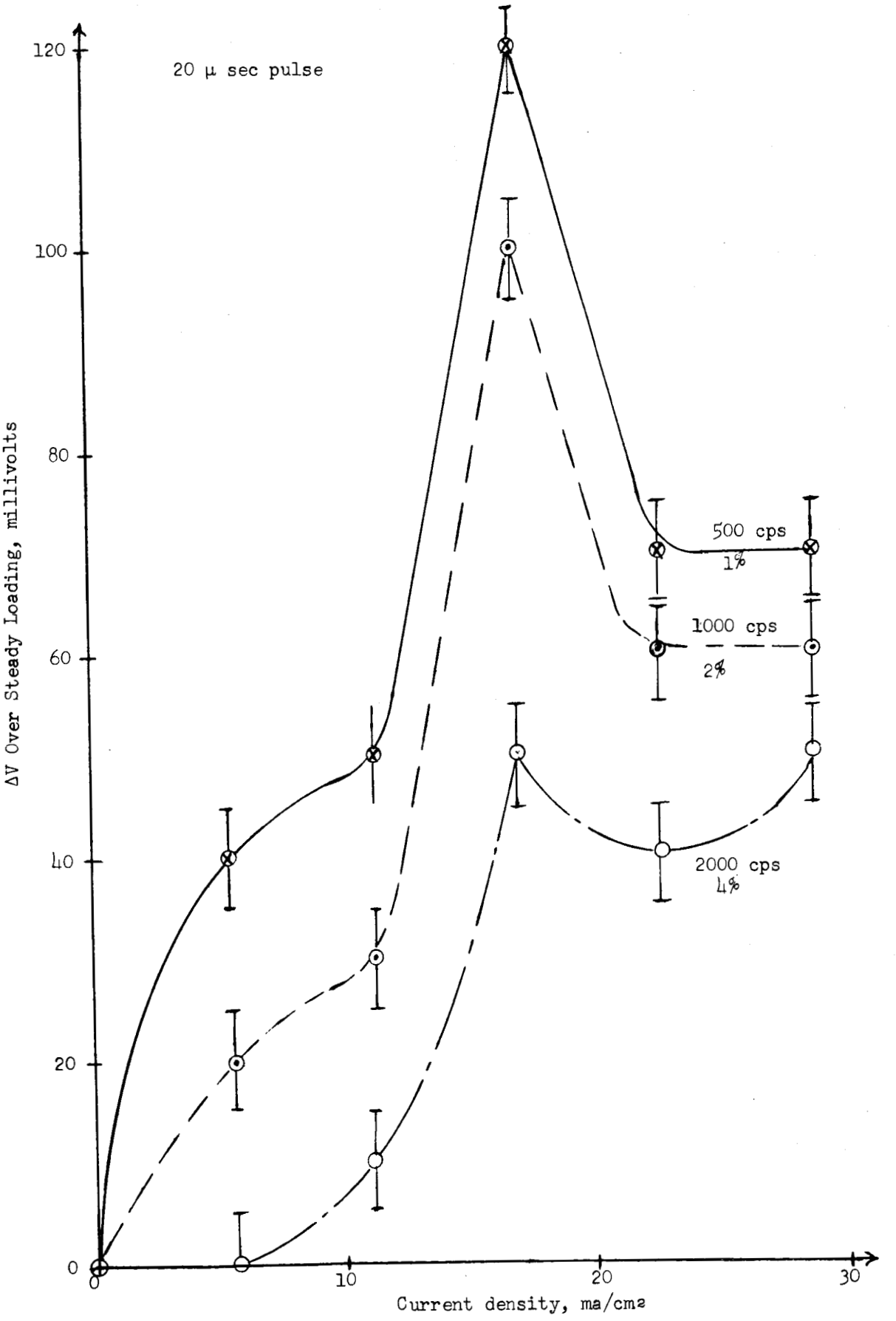

Figure 3. Gain in Voltage under Pulse Loading.

The electrode reaction occurring at the hydrogen electrode in potassium hydroxide electrolyte would be:

$$1/2\ H_2 + OH^- \rightleftarrows H_2O + e^- \ . \qquad (1)$$

The potential of the electrode is dependent on the pressure of hydrogen at the reaction site (which is assumed to be relatively constant), and the activity of the hydroxyl ion. As the concentration of the hydroxyl ion is depleted in the vicinity of the reaction sites at the gas-solid-electrolyte interface, the potential of the hydrogen electrode will become more positive according to the Nernst equation:

$$E_{a_1} = E^\circ - 0.059 \log P_{H_2}^{1/2}\ a_1 OH^- \qquad (2)$$

$$E_{a_2} = E^\circ - 0.059 \log P_{H_2}^{1/2}\ a_2 OH^- \qquad (3)$$

$$\Delta E_{a_1 a_2} = E_{a_1} - E_{a_2} = 0.059 \log \frac{a_2 OH^-}{a_1 OH^-} \qquad (4)$$

where E_{a_1} = potential at a_1 (a_1 is activity for OH^- in asbestos matrix),

E_{a_2} = potential at a_2 (a_2 is activity for OH^- at electrode surface),

E° = standard state potential.

As a_2 approaches zero, E_{a_2} of the electrode changes very rapidly and the current density at the electrode approaches the limiting current density. The equation relating ΔE or electrode concentration polarization to the current density and the limiting current density is well known[1]:

$$\Delta E = \frac{2.3R}{nF} \log \frac{I_L}{I_L - I} \qquad (5)$$

where I_L is the limiting current density and I is the current density at the electrode.

Electrolyte concentration polarization at the hydrogen electrode as a function of current density has been calculated and is illustrated in Figure 2 for both I_L = 20 ma/cm^2 and I_L = 25 ma/cm^2. Again, these calculated curves assume no other polarizing factors are operating. It can be seen from comparison of the experimental curves and the theoretical curve for I_L = 20 ma/cm^2 that the maximum gain in potential from pulse loading (at 500 cycles/second, 1% duty time) observed at 17.1 ma/cm^2 cannot be due to an electrolyte concentration effect alone, but may be partly attributable to it; the ΔE for concentration

polarization at 17.1 ma/cm^2 is 0.050 volt as compared to an experimental depolarization on pulsing of 0.120 volt. As previously stated and as is seen in Figures 2 and 3, the amount of depolarization appears to be dependent on both the frequency of the pulse and the per cent duty cycle. Actually only the per cent duty cycle is important as shown in Figures 4 and 5 where the cell voltage under load is independent of the frequency of the pulse. Figure 6 illustrates the dependence of cell voltage on duty cycle at constant frequency. Discharge curves (Figure 2) appear to be pulse frequency dependent only because the duty cycle is changing.

In order to obtain the same average current density output for the fuel cell at two different duty cycles (1% and 2% at 500 cycles/second and 1000 cycles/second, respectively), the lower duty cycle pulse must carry a higher polarizing current which is on for a shorter period of time and, hence, off for a longer period of time. Factors responsible for the increase in cell voltage under pulse loading at this average current density are difficult to assess in the system employed. If an electrolyte concentration effect is partially responsible, then the following arguments would apply.

The overall cell voltage depends on a difference between a positive potential on the oxygen electrode and a negative potential on the hydrogen electrode. Here we are considering the potential of the oxygen electrode constant. Hence, the cell voltage varies only with the potential of the hydrogen electrode. The more negative the potential of the hydrogen electrode, the greater the cell voltage. If only electrolyte concentration polarization is affecting the electrode potential, then from equations (2) and (3) it can be seen that the potential is dependent only on the activity of the hydroxyl ion.

On 100% duty time the potential remains constant for a particular current density and corresponds to a certain activity a_1 of hydroxyl ions at the reaction sites. When a pulse of short duty cycle is applied to the electrode to produce the same average current density, the polarizing current is considerably higher. Therefore, during the pulse, hydroxyl ions are rapidly used up in the vicinity of the reaction site. The activity of the hydroxyl ions at the end of the pulse would be considerably lower than a_1. When the load is released, however, a buildup of hydroxyl ions at the surface commences. The rate of buildup must be high enough to produce a high activity of hydroxyl ions at the end of the off cycle. The average activity of the hydroxyl ion during the cycle must be higher than the average activity at the electrode to produce a higher voltage for the cell. For a 1% duty cycle, the load is off 99% of the time. The rate of replenishment of hydroxyl ions would have to be only a fraction of the rate of depletion on the load cycle to produce an average activity which would be greater than that for 100% duty cycle.

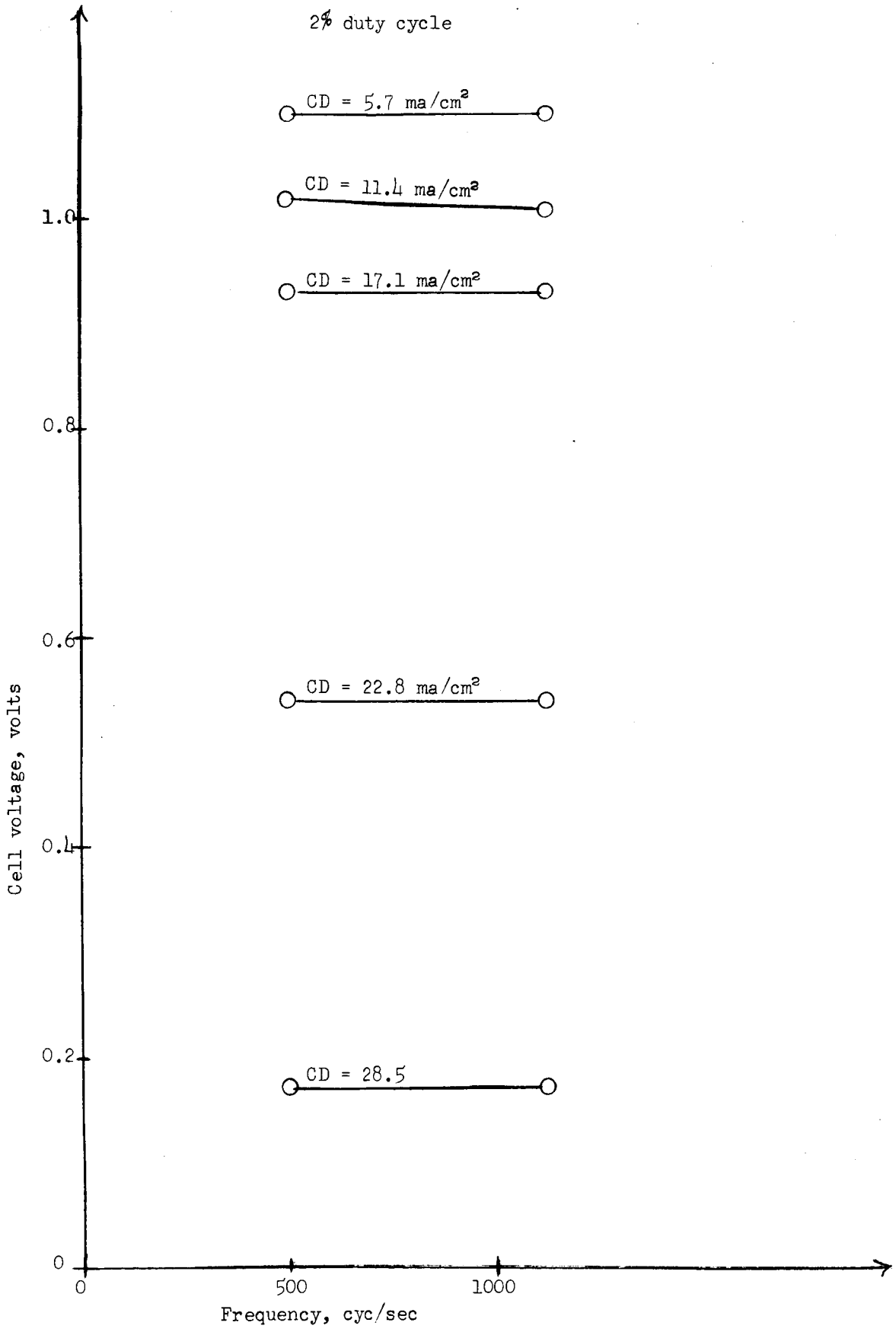

Figure 4. Dependence of Cell Voltage on Pulse Frequency.

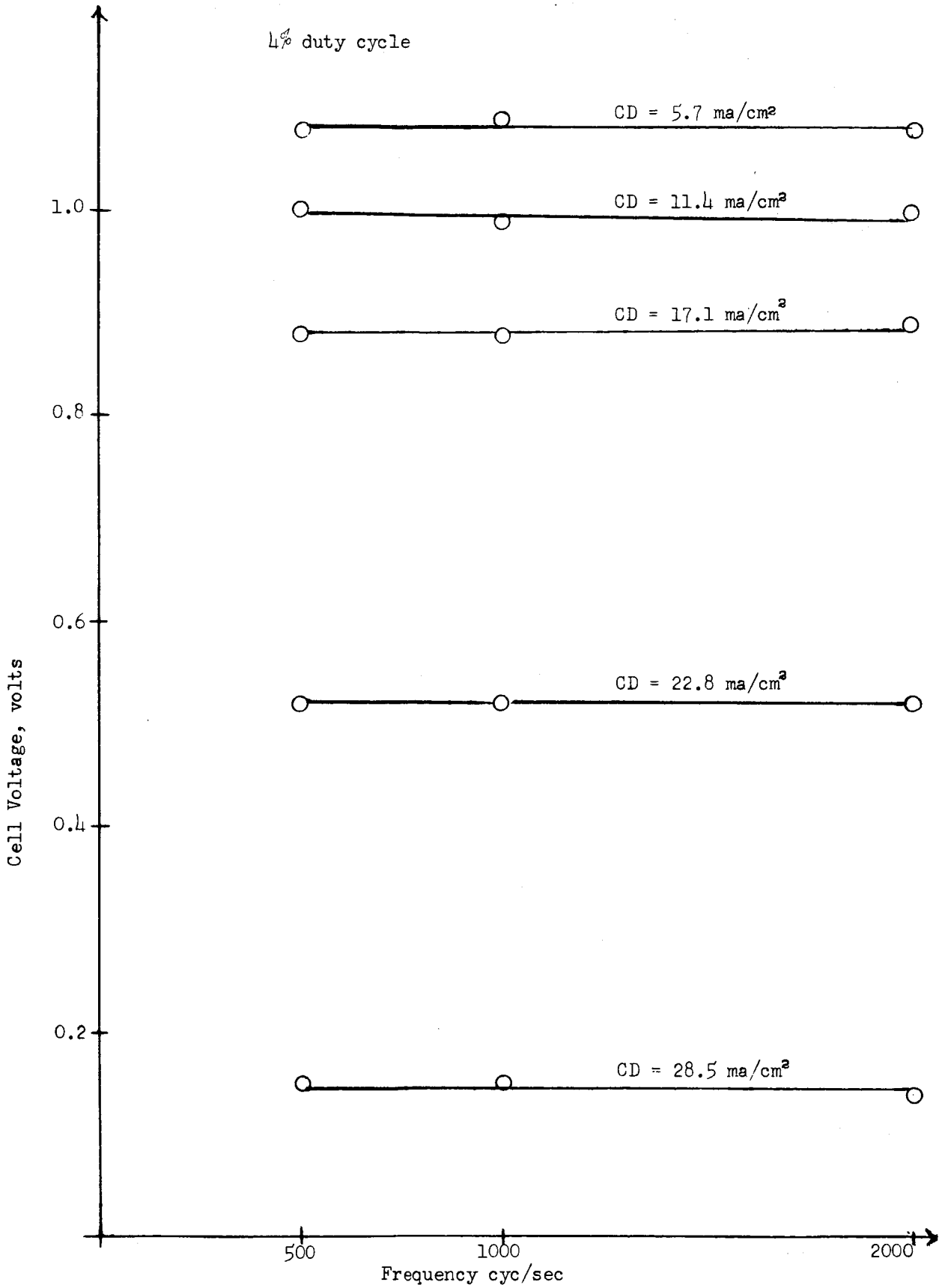

Figure 5. Dependence of Cell Voltage on Pulse Frequency.

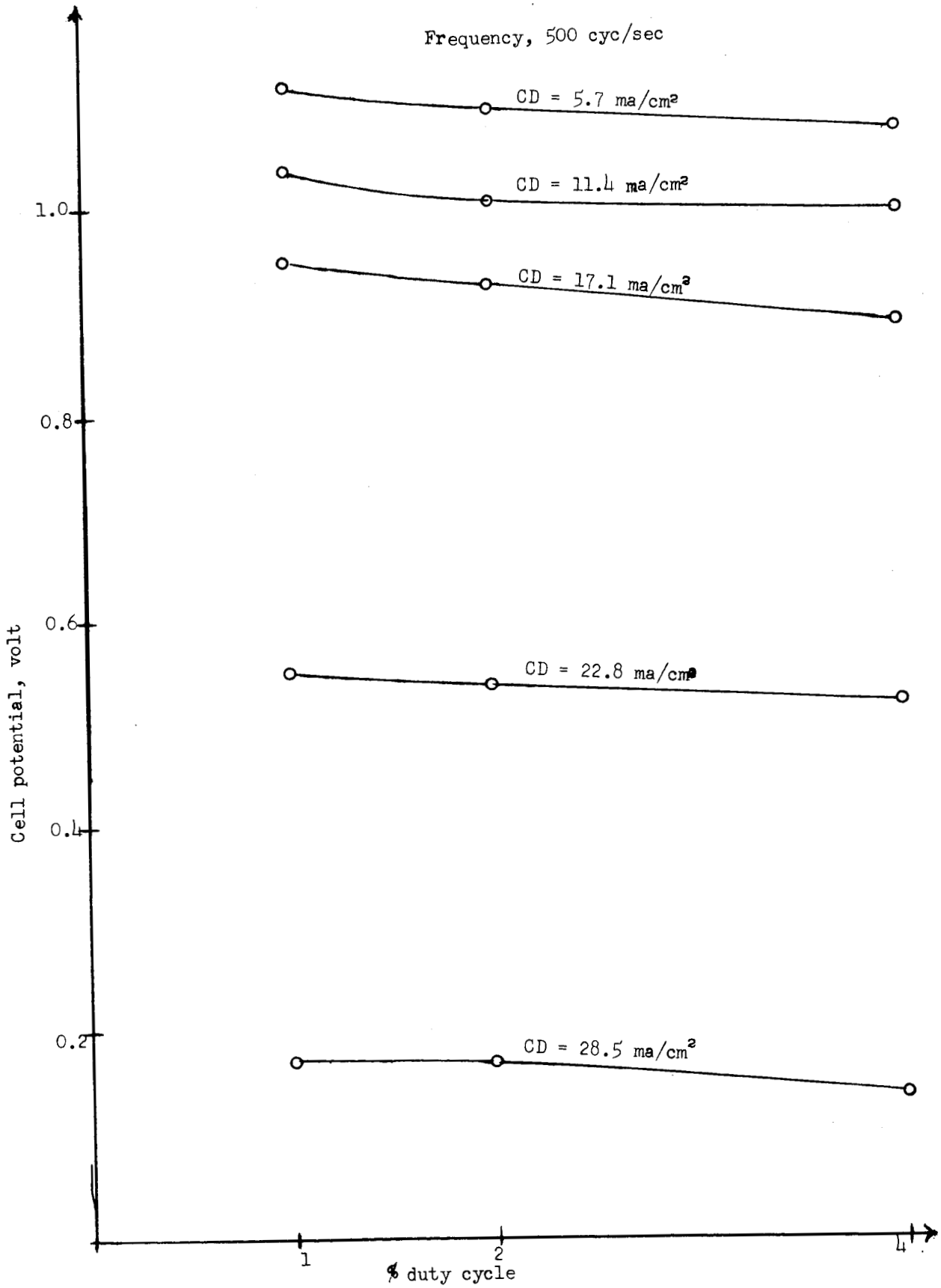

Figure 6. Dependence of Cell Voltage on Per Cent Duty Cycle at Constant Frequency.

Application of mathematical methods of analysis to support this theory are in a first stage and will not be pursued further in this report. However, the effect of pulsing on concentration polarization must be assessed in an aqueous electrolyte system and studied on a simple, single electrode if the results are going to be meaningful toward the applications of methods of analysis.

Concentration polarization does not appear to be the entirety of the depolarizing effect from pulse loading as is illustrated from Figure 2 where a comparison of the theoretical and experimental curves is given. Ohmic and/or activation depolarization must contribute to the increase in cell voltage. With the present data, there is no way of determining how these are affected by pulsing. If the depolarization is primarily due to ohmic reasons, the average internal resistance of the fuel cell during pulsing must be lower than on steady load. Depolarization of a fuel cell due to a lowering of the internal resistance under pulse loading could result in considerable gain in power for high power output cells. The effect, however, needs to be studied in considerable detail to be well defined.

Figure 7 clearly illustrates the increase in power output of the fuel cell at 1% duty cycle. The voltage vs current density, and discharge curves for 40 and 80 microseconds duty times are illustrated in Figures 8 and 9, respectively. Various frequencies of the pulse are noted. Comparing these figures and Figures 10 and 11 with those for a 20 microsecond duty time it is easily seen that the gain in power output of the fuel cell from pulse loading decreases with increasing duty time at constant frequency. Thus, as stated previously, the advantages from pulse loading increase with decreasing per cent duty cycle. Longer duty cycles than these were studied but without any apparent gain in power output. In order to study shorter duty cycles, the pulsing circuit must be modified to accommodate the higher current loading that is necessary.

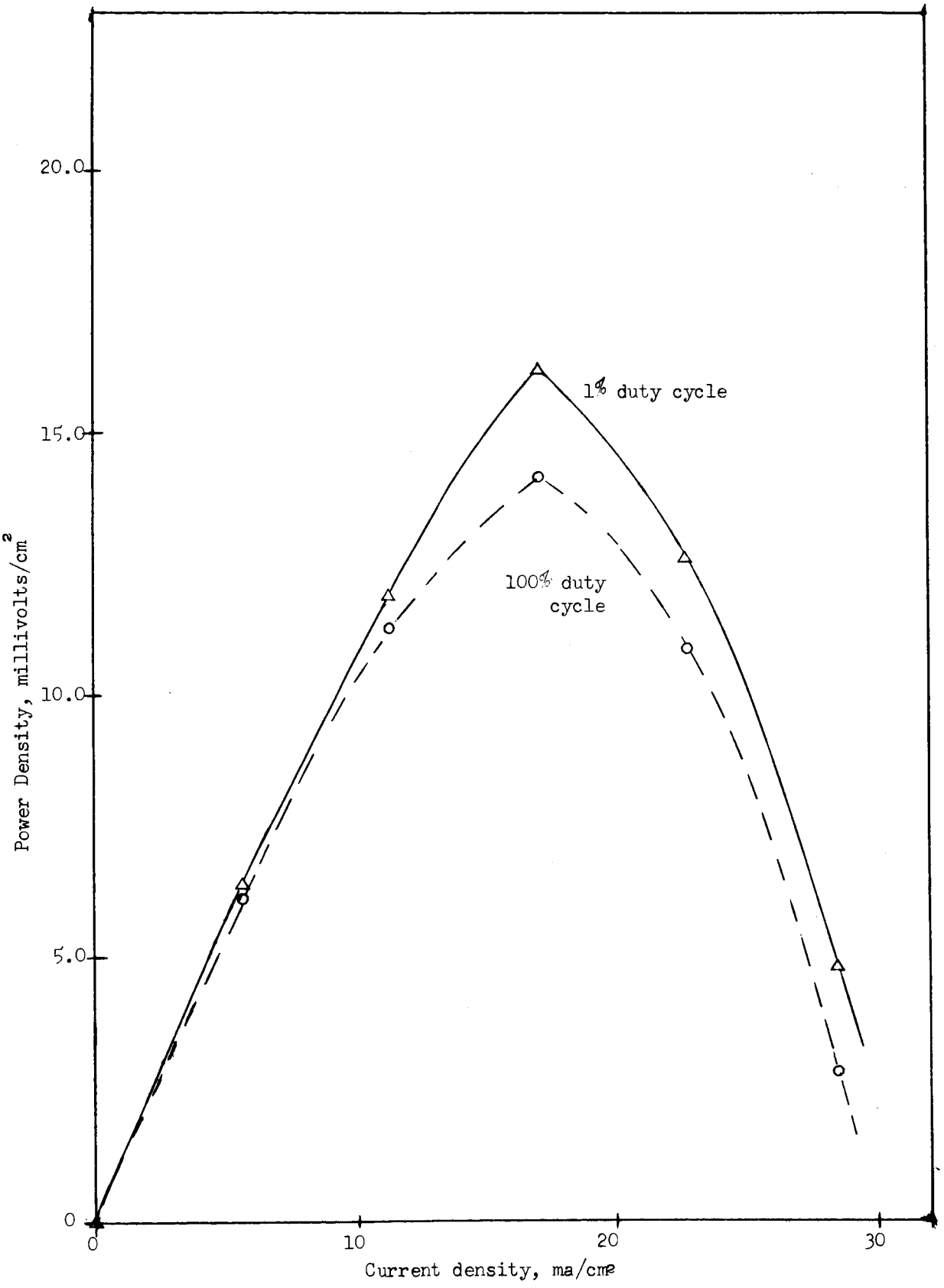

Figure 7. Power Density of Fuel Cell on Pulse Loading.

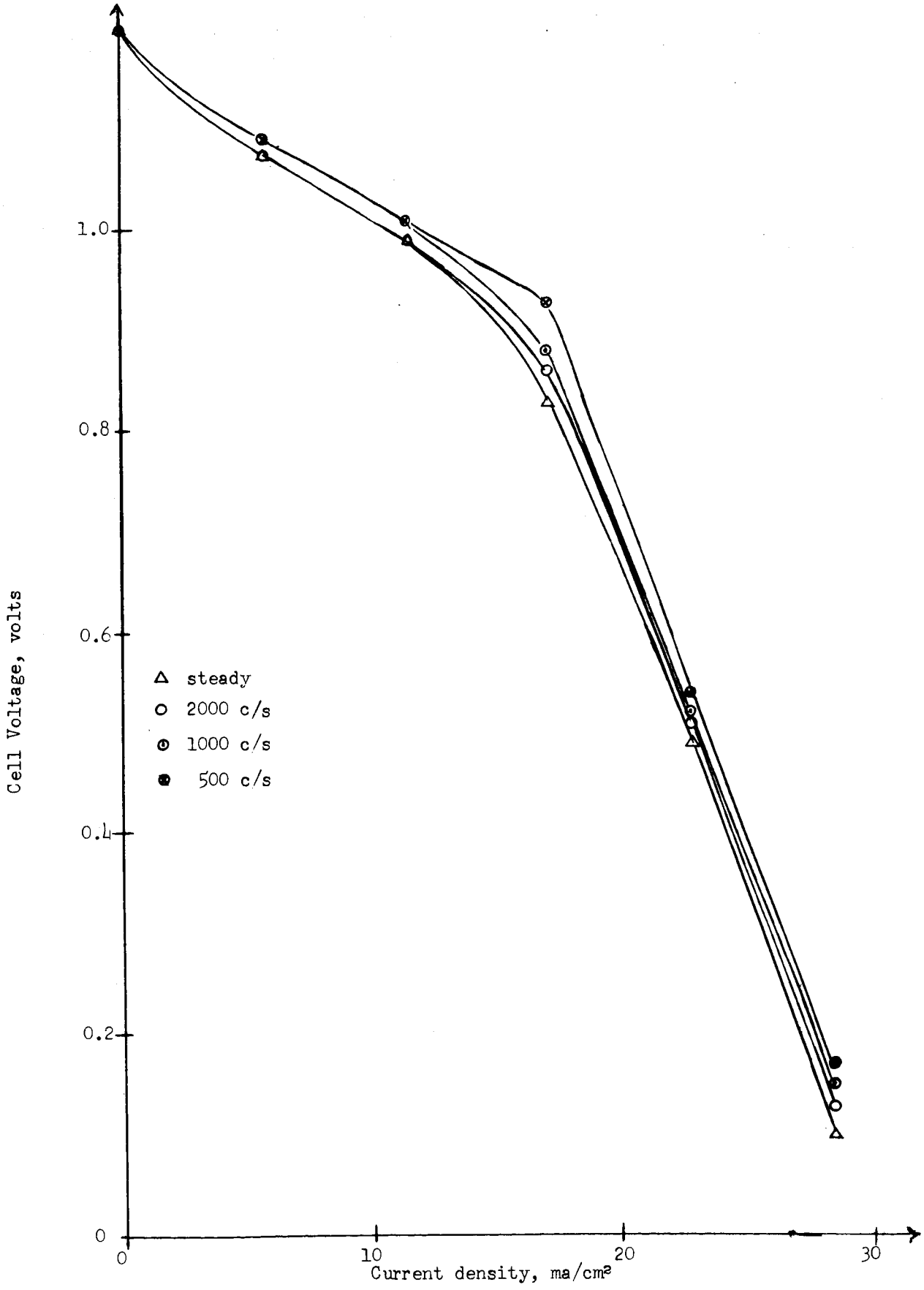

Figure 8. Discharge Curve for 40 Microsecond Duty Time.

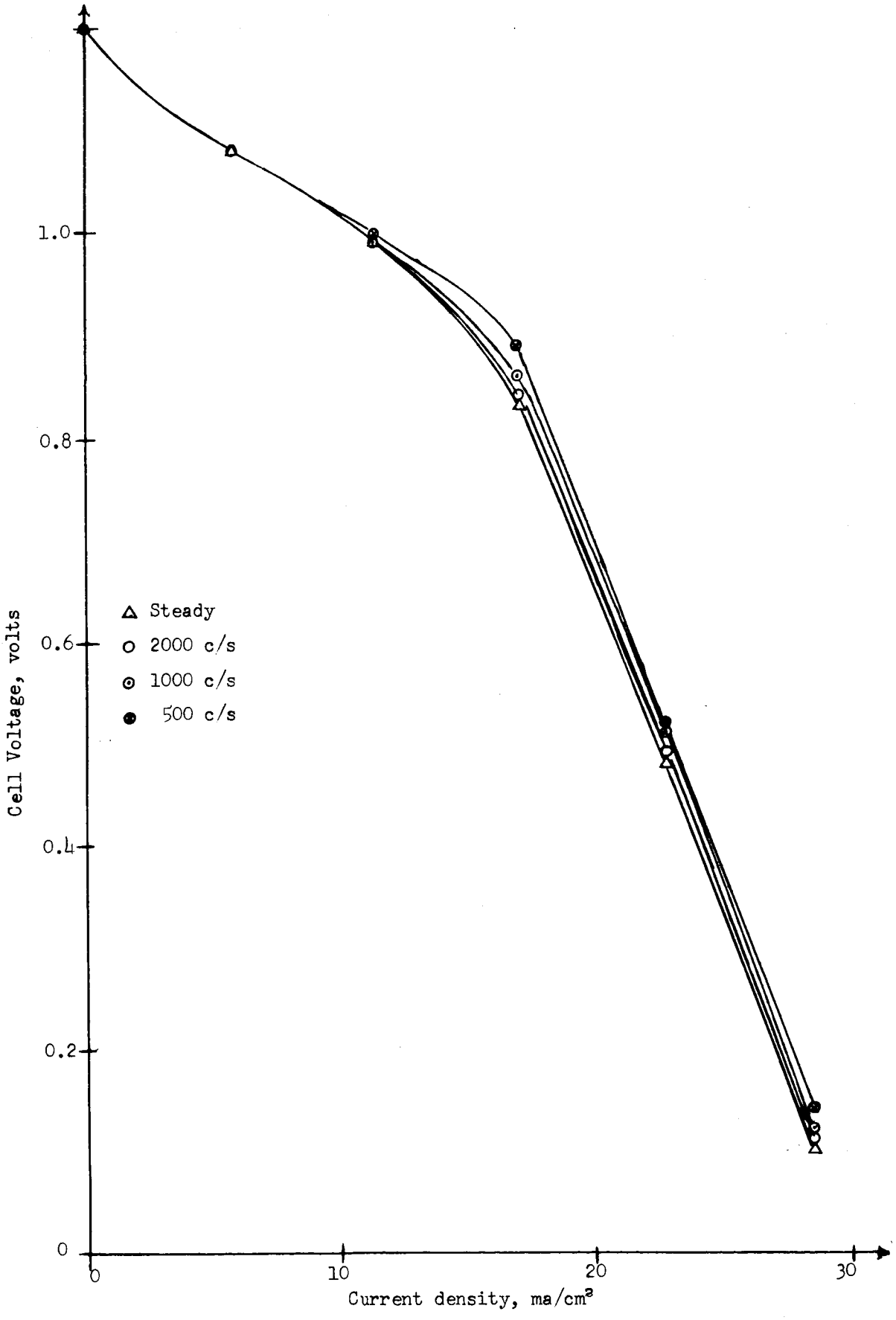

Figure 9. Discharge Curve for 80 Microsecond Duty Time.

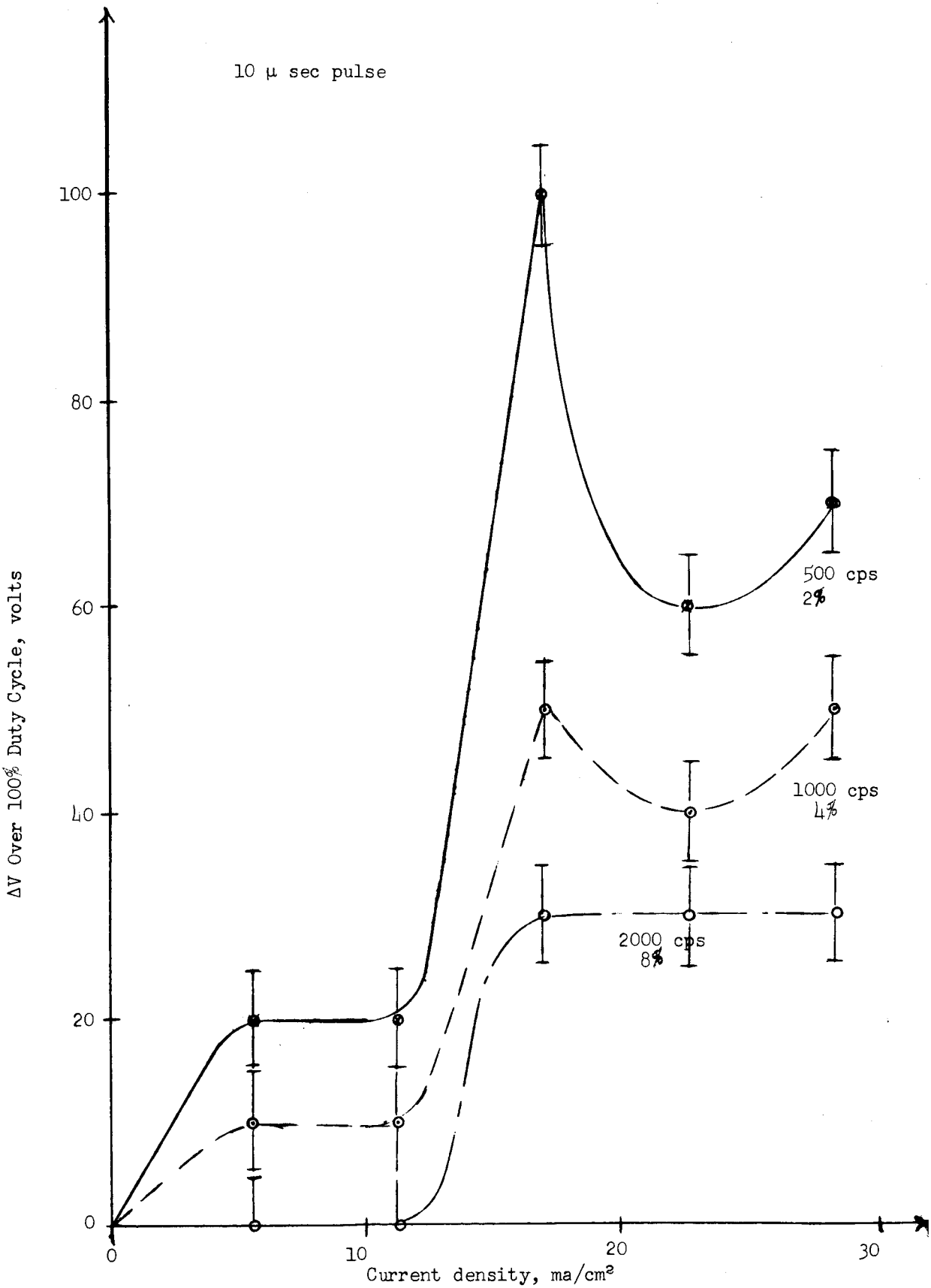

Figure 10. Gain in Voltage on Pulse Loading.

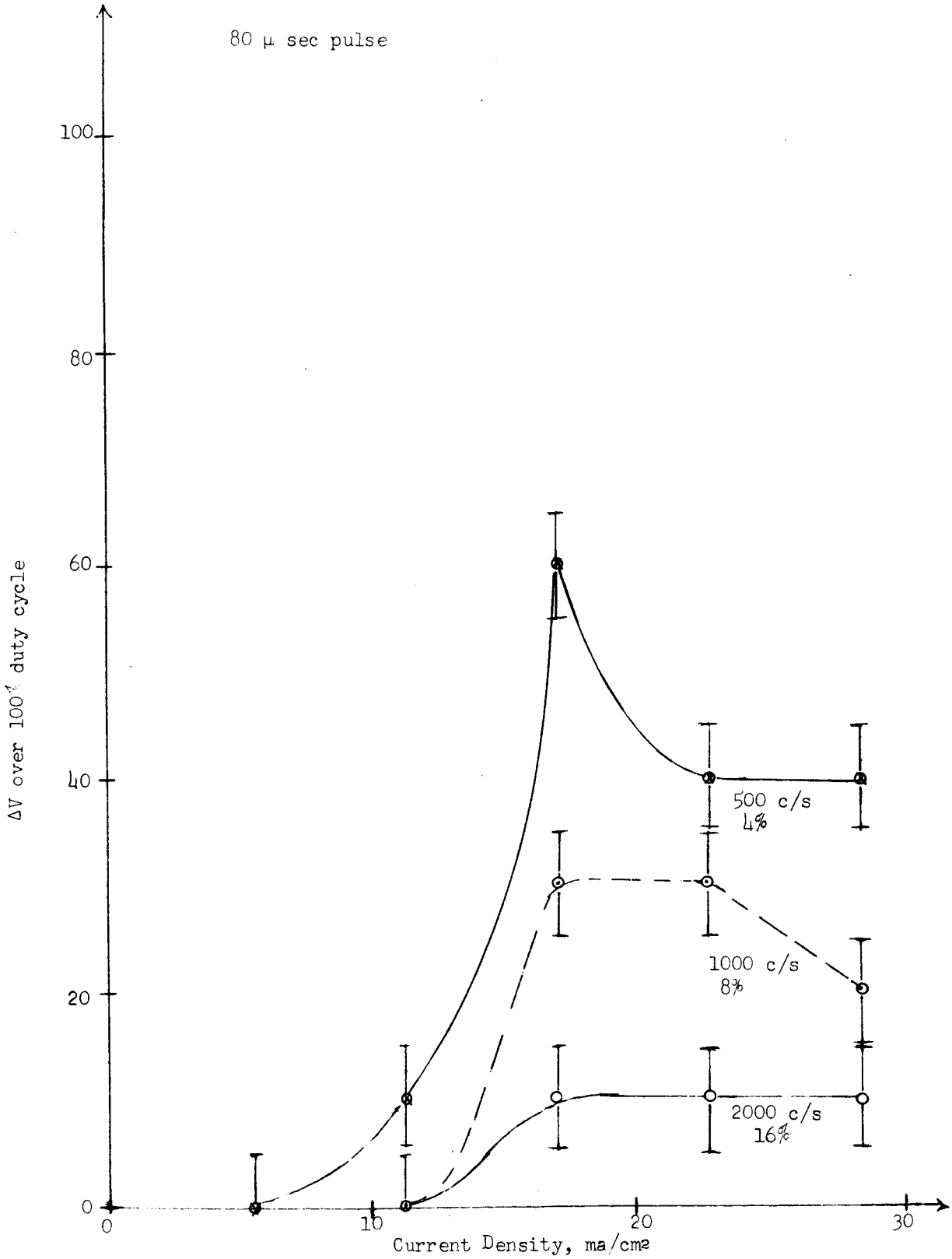

Figure 11. Gain in Voltage on Pulse Loading.

PULSE CIRCUIT UNDER CONSTRUCTION

The pulse loading circuit shown in Figure 1 contains certain limitations, the most obvious of which is the power consumed by the 2N2152A power transistor and the 1N1204 diode under very high currents. Large currents are necesssry to study even very small cells at low percentage duty cycle. For example, to draw 100 ma average current from a cell at 1% duty cycle, a current of 10 amps must flow through the transistor and diode during the time the transistor is on; at this high current the potential drop across the transistor and diode is appreciable. To compensate for this, a d.c. power supply of high voltage may be employed but the voltage may not be higher than the maximum emitter-collector rating on the transistor (in the case of the 2N2152A, 45 volts). The new pulse loading system now being built would eliminate much of the problem by replacing the transistor with a silicon controlled rectifier, the internal resistance of which is very low.

The purpose of the new circuit, shown in Figure 12, is to study actions of multiple fuel cells under conditions of heavy load at 33-1/3% duty cycle at design frequencies of 400 to 1000 cps in steps of 100 cps.

Circuit description: Momentary contact of SW1 applies a positive potential to the gate of CR1, causing the device to conduct and impress the d.c. potential of fuel cell #1 across the primary of T1. T1, T2, and T3 are step-up transformers in a ratio of 1:18, so the rate of change from zero volts to average fuel cell voltage is detected and amplified by transformer action. At T1 secondary it is further rectified and clipped by D5 and D4 to produce a voltage across the load, reference voltage across R7, Z1, and P1, and a charging voltage for phase #2 across R1, R4, FR1, RX1, and C2 of the timing circuit. Switch #3, a ganged rotary switch, is adjustable to give a firing range of 400 to 1000 cps -- frequency specifications of the transformers. RX1, RX2, and RX3 are firing calibration resistors to equate the breakdown voltages of Q1, Q2 and Q3 for exact timing of the circuit. When breakover voltage is reached on the emitter as compared to a common reference voltage on base 1 of Q1, C2 discharges through base 2 of Q1, developing a negative pulse on the base of Q4. This switches a positive pulse on the collector of Q4 which in turn supplies the necessary potential to turn on CR2 and back bias CR1 through D1 into a non-conducting state. When CR1 turns off, the first timing circuit no longer has charging voltage and will revert to a non-conducting state the instant CR1 is back biased. When CR2 turns on, charging voltage enters D6, R2, R5, FR2, RX2, and C3 and the second timing circuit generates a timed potential to turn on CR3 and turn off CR2. The action of CR3 and the third timing circuit is identical, and a complete three-phase firing pattern is developed.

For satisfactory operation, this circuit requires a minimum of 1.2 volt at each cell position under maximum load conditions. Transformers $T_{4,5,6}$, 6 volt primary, 115 volt secondary, 60 to 2000 cycle.

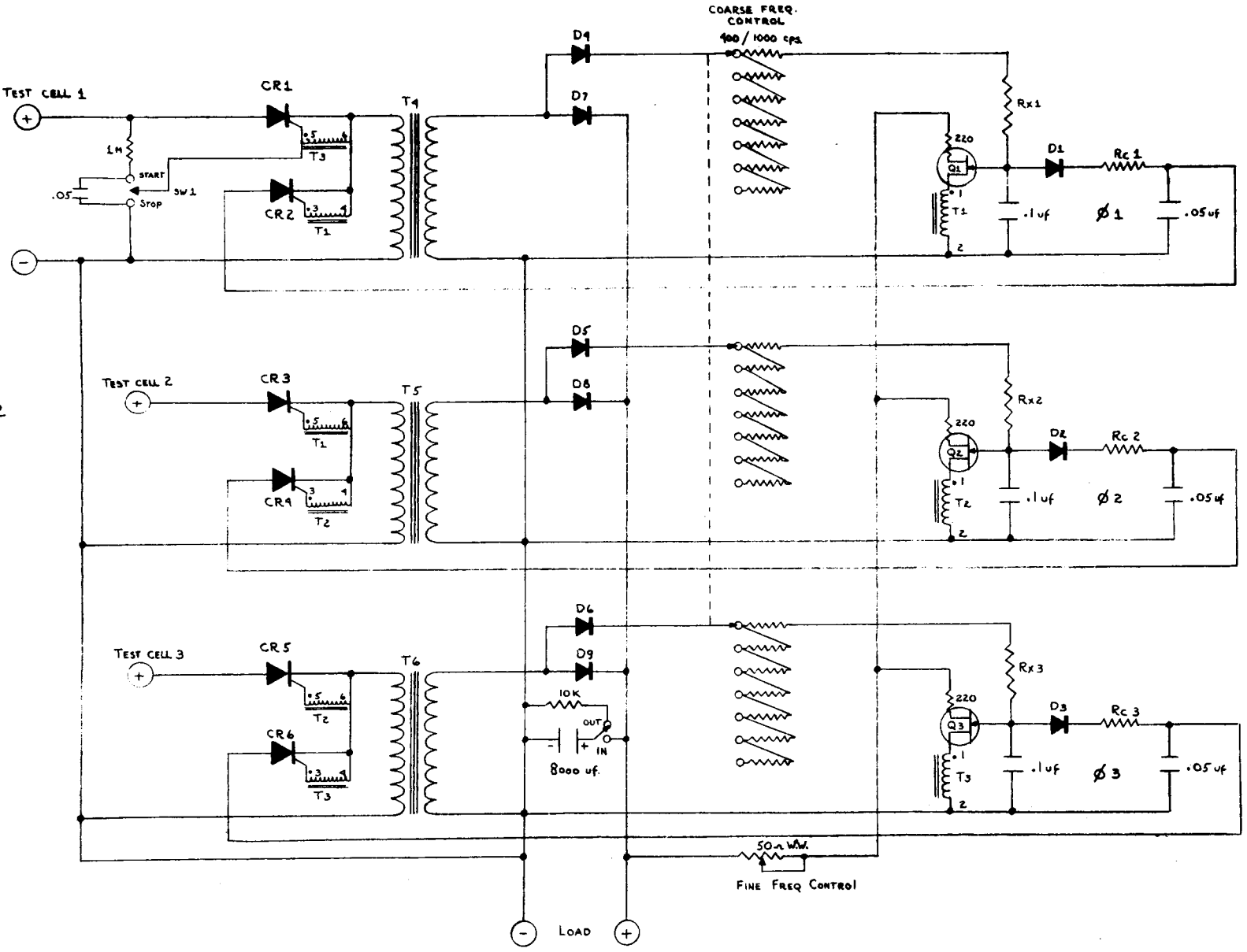

Figure 12. Circuit Diagram for 3-Phase Fuel Cell Analyzer.

3 PHASE TEST CELL ANALYZER	
NASA	PROJECT
ALFRED	UNIVERSITY
Dr. T.J Gray	

Reference voltage is made adjustable in the laboratory model by P1 to attain the maximum efficiency of the fuel cells under test. If the load is large enough so that the cells do not recover sufficiently during the rest period to maintain a voltage across the charging circuits greater than or equal to the voltage at P1, the charging circuits will cease to operate. Additional information on fuel cell decay may be extracted at this load by adjusting potentiometer P1 until the reference voltage level is less than the charging voltage. This resumes circuit function until the cells are no longer able to supply significant outputs.

SW2 cuts a large filter capacitor, C1, out to aid in the study of the fuel cell decay curves, and in, to give a smoothing action for a d.c. load if desired.

Work has already begun on a possible modification of the circuit discussed above which will enable each of the SCR's to be turned off at will anytime before the next one fires. In this way, the fuel cell can be studied at a percentage duty cycle much lower than 33-1/3%.

The obvious advantage of the new circuit is that, disregarding any power increase due to pulsing, there is an improvement in the form in which power from the cells is delivered. Instead of low voltage direct current, a three-phase alternating current is available which can be transformed or rectified at will.

PART II

GALVANOSTATIC INVESTIGATION OF FUEL CELL ELECTRODES

INTRODUCTION

In conjunction with experiments on the anodic behavior of palladium-gold alloy wires in H_2SO_4 electrolyte[1], efforts were made to reproduce the results of other investigations on gold[4,5,6] at varying polarizing current densities. The data obtained lend support to a mechanism proposed by Armstrong, Himsworth and Butler[5] that the formation of Au_2O_3 occurs throughout the formation of a chemisorbed oxygen layer on the gold surface. According to potential data reported in the literature[4,5,6] the conversion of the oxide layer to Au_2O_3 is shown to be that of the electrochemical conversion of Au_2O to Au_2O_3, occuring at 1.24 volts. Further, it has been found that at current densities of the order of 0.2 ma/cm^2 or lower, the reaction occurring at this potential can be sustained for long periods of time (ca 24 hours). It is proposed that some of the Au_2O_3 formed electrochemically must decompose to reform the reactant and oxygen to maintain this potential. The Au/Au_2O_3 oxidation is well defined at 1.36 volts at a range of current densities (10 μa/cm^2 to 10 ma/cm^2). The formation of the lower oxides of gold, Au_2O and AuO, as reported by El Wakkad and El Din, is not detectable until very low current densities are reached.

EXPERIMENTAL ARRANGEMENTS

High purity (99.9%) gold wire (0.01 cm diameter) was obtained from Engelhard Industries. The wire was cut in lengths which when sealed in capillary tubing would allow a 10 cm coil to be exposed to the electrolyte. A seal of Silastic RTV (Dow Chemical) silicon resin was employed between the tubing and the gold. Contact with the external polarizing circuit was made directly through the wire.

An all-glass, U-type electrolytic cell was employed with the two compartments separated by a fine fritted disc to prevent mixing. The lower part of the compartment which held the gold electrodes was connected externally through another fine frit to a valve through which nitrogen could be admitted. The upper portion which held the gold electrode and the reference electrode was connected to the compartment by a ground glass fitting.

The electrolyte was high-purity H_2SO_4 diluted to one normal with distilled water. The acid was boiled to deoxygenate and cooled in the electrolytic cell under an atmosphere of high-purity nitrogen before each experiment. Immediately before the electrode was introduced into the cell, the gold wire was polished with filter paper, dipped in dilute HCl for 15 minutes and rinsed in distilled water.

Platinized platinum served as the counter electrode. The reference calomel electrode was connected to the gold electrode compartment by a KCl bridge drawn to a fine capillary. The potential of the reference electrode was checked periodically by comparison with another saturated calomel electrode.

The U-tube assembly was immersed in a water bath and a temperature of $25 \pm 0.05^{\circ}C$ was maintained for all experiments. A precision, constant-current generator in the external circuit was used to polarize the electrodes and current was read on a 0.5% milliammeter. The change in potential of the electrodes was followed with a recording Corning solid-state electrometer having an input impedance of 10^{13} ohms. Hence, current drawn by this source was negligible. A high-speed, 10 millivolt recorder on the electrometer was calibrated continuously against the electrometer. Potential of the gold electrode against the reference calomel was recorded at constant polarizing current. All potentials reported in the text are reported on the scale of the normal hydrogen electrode.

RESULTS

Charging Curves

Anodic charging curves were run on numerous gold wire samples at a wide range of current densities. One important phenomenon was observed on all the wires; the first-run potential curve on each was different than subsequent curves. Curves I, II, and III of Figure 13 are typical. When the electrodes were immersed in the electrolyte initially the potential was ca 0.4 volt. Cathodic polarization, even at current densities less than 1 ma/cm^2, produced a hydrogen overvoltage greater than 0.13 volt (curves I and II). Reversal of current led to (a) a rapid linear drop in potential with time which has been attributed to the charging of the electrical double layer, (b) an arrest beginning at 1.30 to 1.36 volts after which two kinds of behavior were observed. At low current densities, a drop in potential was observed with the potential becoming relatively constant at about 1.25 volts (curves I and II). Higher current densities, however, polarized the electrode directly to the oxygen evolution potential (curve V). Subsequent anodic charging curves, after cathodic polarization to hydrogen evolution, were reproducible following either curve I or II of Figure 2 depending on the current density. In curve I of Figure 14, an initial linear, potential vs time, double-layer charging region preceded two arrests in the curve; the latter indicating two different electrochemical processes occurring. The first arrest was at ca + 1.24 volts and the second began at ca + 1.35 volts. At lower current densities (curve II of Figure 14), the potential did not exceed that of the first electrochemical reaction. The electrochemical reaction could be sustained at this potential on gold wires for as long as 24 hours. No longer runs were made. Subsequent cathodic charging curves show a single arrest at + 1.04 volts (Figure 14, Curve II), a potential slightly more negative than the potential of the anodic reaction. After a linear double-layer charging region, another small arrest was observed at ±0.1 volt before hydrogen evolution occurred. Hydrogen overvoltages here were lower than on the first runs.

Figure 14, curve Ic, shows the cathodic charging curve following anodic polarization to oxygen evolution. A linear drop in potential is interrupted by two arrests; one at a potential of 1.16 volts and a second at 1.04 volts. The latter corresponds to the potential of the arrest in the cathodic portion of curve IIc (Figure 14). Again a distortion of the linear double layer charging line is seen at +0.1 volt before hydrogen evolution occurs.

Decay Curves

A typical decay curve, from the oxygen evolution potential, is shown in Figure 15. Following an initial fast drop in potential, arrests occur at ca 1.36 volts, 1.24 volts, and 0.36 volt.

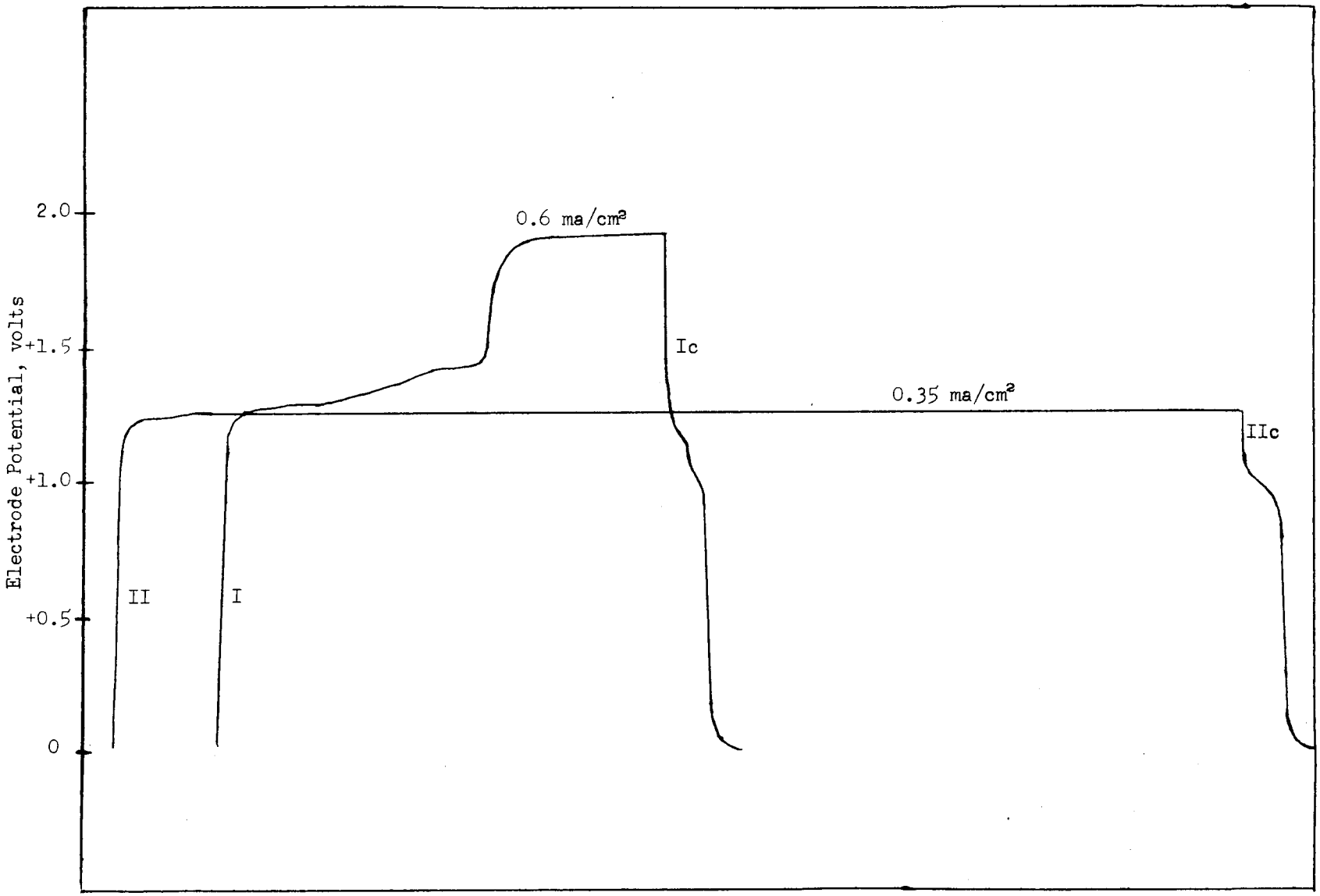
2.0
+1.5
+1.0
+0.5
0
Electrode Potential, volts
0.6 ma/cm²
Ic
0.35 ma/cm²
IIc
II
I

Figure 14.

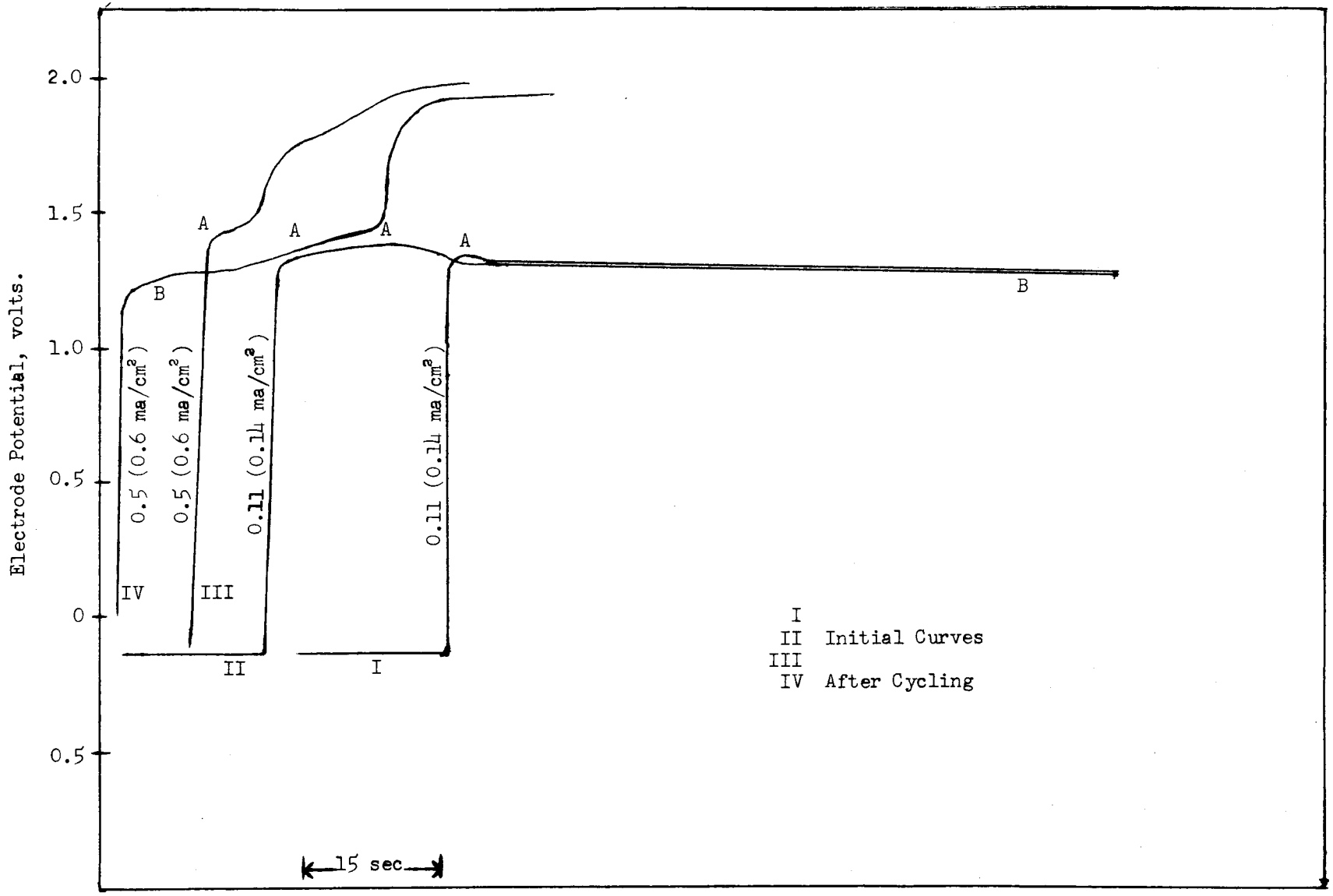

Figure 13. Anodic Oxidation of Gold Wire.

DISCUSSION

Anodic charging curves show that no hydrogen ionization step is observed on the gold electrodes in a 1N H_2SO_4 electrolyte, a phenomenon which is distinctly different from that on platinum and palladium[2,3] but has been found by other investigators[4,5,6]. The lack of a hydrogen ionization step on gold indicates that an undetectable amount of hydrogen is sorbed when hydrogen is evolved during the previous cathodic polarization process. Similar results have been found with gaseous hydrogen on gold, since no chemisorption is detectable up to 0°C[6]. Gold electrodes, charged with gaseous hydrogen, have been found to generate a potential of 0 volt[8], which presumably would result from hydrogen chemisorption. However, decay curves for gold electrodes electrolytically charged with hydrogen indicate very little ionizable hydrogen on the gold surface.

Calculation of the capacitance of the electrical double layer from the linear portion of the anodic charging curves gave values which ranged between 125 and 300 microfarads. Although the capacitance appeared to increase with current density, the effect does not appear to be well defined. A value of 200 microfarads is taken as an average value.

Since the apparent area of all the electrodes used in this investigation was 0.8 cm^2, the double-layer capacitance per apparent square centimeter would be 250 microfarads. If the value of 100 microfarads per actual square centimeter of area is accurate[6], then the area of the gold electrode is 2.5 square centimeters. The number of gold atoms in the surface then is about 3×10^{15} as calculated from the lattice parameter of 4.07 A on an edge of the face centered cube with the (001) crystal plane exposed. The ratio of actual to apparent area, on this basis, is 3:1, a value close to the value of 2:1 taken by Hickling[4] for shiny gold.

The first run anodic charging curves on the gold electrodes in Figure 14 were obtained in freshly deoxygenated electrolyte maintained continuously under nitrogen. Further, the electrode had not been previously polarized to oxygen evolution; hence it is to be assumed that little oxygen is present in the electrolyte. The first-run curves exhibited two types of behavior, depending on the current density employed for the oxidation. At high current densities, a single arrest was observed in the charging curve beginning at greater than 1.30 volts with a temporary plateau reached at 1.36 volts; the potential then increased to a steady value where oxygen evolution occurred. On electrodes where the initial anodic run was made at low current densities, the potential arrest began at greater than 1.30 volts as previously, reached a momentary plateau at 1.36 volts; then the potential dropped to a value of ca 1.24 volts and remained constant. The first electrochemical reaction occurring at ca 1.36 volts has previously been defined[4,5,6] to be the conversion of Au to

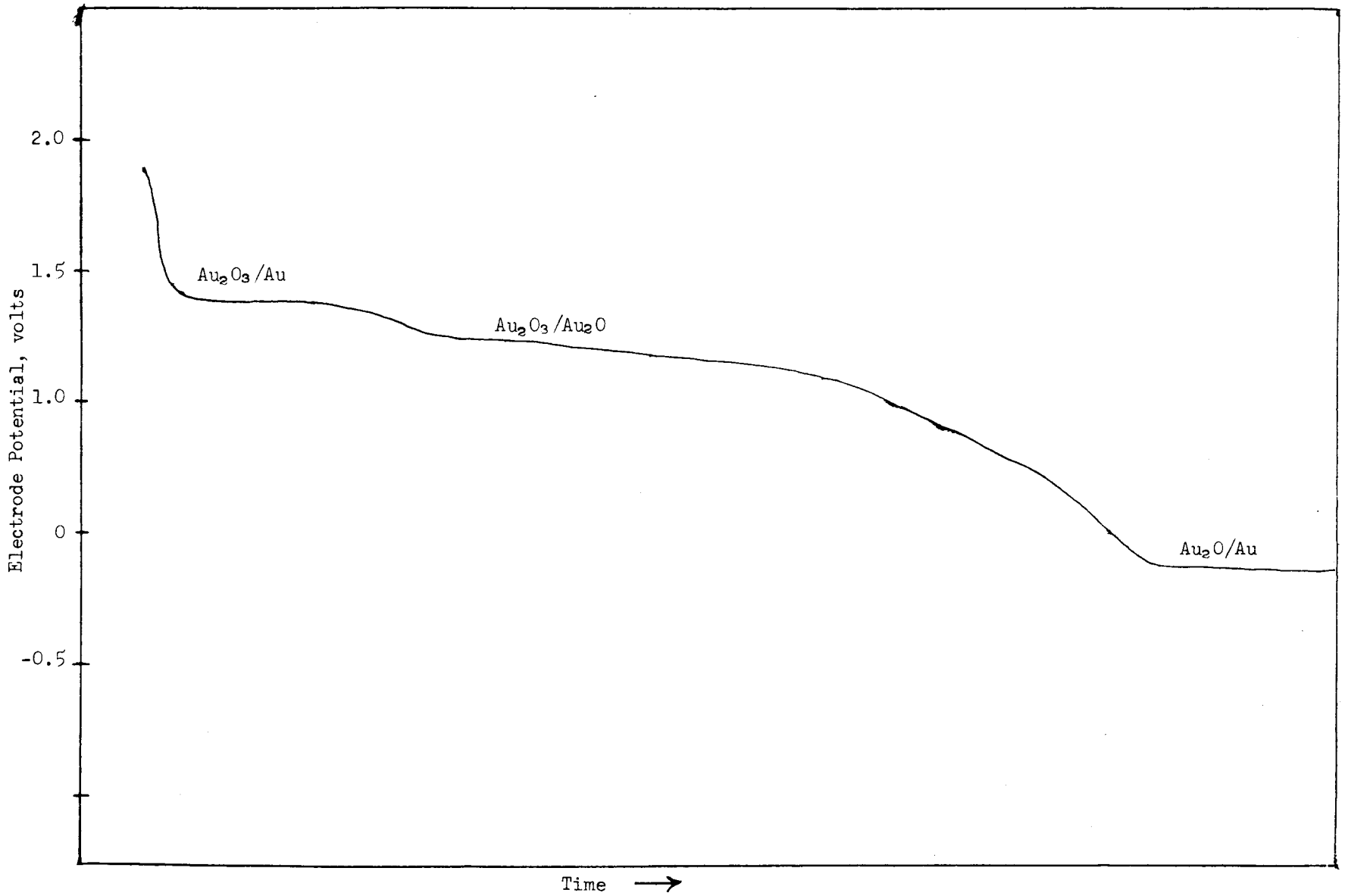
2.0
1.5
1.0
0
-0.5
Electrode Potential, volts
Au_2O_3/Au
Au_2O_3/Au_2O
Au_2O/Au
Time

Figure 15.

Au_2O_3. The reaction occurring to support a potential of 1.24 volts in H_2SO_4 has not been reported. However, a reaction beginning at 1.24 volts on gold has been found by Schmid and O'Brien in $HClO_4$ solution[8]. This reaction was attributed to the oxidation of a chemisorbed layer of oxygen to Au_2O_3 and occurred as the potential gradually increases from this value.

Hickling's results[4] at high current densities indicate only one anodic arrest at 1.36 volts before oxygen evolution. Hence, only the electrochemical conversion of gold to Au_2O_3 was observed. Armstrong, Himsworth and Butler[5] reported an initial distortion of the linear, double-layer charging curve at 1.27 volts with the temporary plateau reached at 1.36 volts before a gradual rise in the potential to oxygen evolution. They proposed that a layer of oxygen atoms were formed initially on the surface which led to the formation of the Au_2O_3.

Two mechanisms were proposed to explain the depolarization processes, one of which was the following:

A monolayer of oxygen was deposited on the gold surface and by rearrangement of the first two surface layers of gold atoms during the electrochemical reaction formed Au_2O_3 (1.36 volts). The gradual increase in potential of the electrode was attributed to the increase in current density at the electrode surface as progressively more electrochemical sites were blocked by the Au_2O_3. Results of anodic curves in this investigation appear to lend support to the mechanism postulated by Armstrong, Himsworth and Butler[5] and the results of Schmid and O'Brien. However, present results show that a sustained anodic electrochemical process is operating at a potential of ca 1.24 volts at low current densities. This potential has been observed to be constant for periods of oxidation up to 24 hours. If the product of the electrochemical reaction is assumed to be Au_2O_3, then either the Au_2O_3 is decomposing to reform the reactant and some other species or passing into solution as Au (III) ions, or both.

El Wakkad and El Din[6] have measured the equilibrium potentials of various gold couples in 0.1N H_2SO_4. Assuming the couples obey the Nernst equation, they would be for a 1N H_2SO_4 solution:

Couple	Equilibrium potentials
Au/Au_2O	0.42
Au/AuO	1.04
Au/Au_2O_3	1.36 v.

The results of their investigations of the gold surface by methods of anodic charging curves at very low current densities show that these three oxides are formed at the surface.

Employing the measured values of the equilibrium potentials, the standard state value of the Au_2O/Au_2O_3 couple in 1N sulfuric acid was calculated to be about 1.23 volts. The potential is similar to that observed in this investigation for the electrochemical reaction at 1.24 volts. In the first-run potential curves this reaction did not occur until some Au_2O_3 was formed at 1.36 volts after which the potential dropped to 1.24 volts and remained constant at low current densities. The electrochemical reaction occurring at 1.24 volts, then, appears to be established through Au_2O_3, possibly by decomposition. At higher current densities, the drop in potential is not observed but rather the electrode is polarized directly to oxygen evolution. Since all anodic charging curves subsequently show a reaction occurring at ca 1.24 volts, it would appear that the reaction is limited either by oxygen in the solution, produced by evolution or by the decomposition of Au_2O_3. The latter reaction could occur by the following mechanism:

$$(1) \quad Au_2O_3 \rightarrow Au_2O + O_2$$

followed by electrochemical reaction:

$$(2) \quad Au_2O \rightarrow Au_2O_3 .$$

Thus, the potential at 1.24 volts could be sustained.

An alternate mechanism which could be operating is that the Au_2O_3 is dissolving in the electrolyte as it is produced. Analytical evidence has been found which would substantiate this theory. After oxidation at low current densities (1.24 volts) for times greater than four hours, colorimetric analysis for gold in the electrolyte showed positive results upon reduction of the solution with Hg_2Cl_2. It is unlikely, however, that this is the entirety of the reaction occurring. In order to support proposed Au_2O/Au_2O_3 reaction at 1.24 volts on the first-run potential curve, presumably Au_2O_3 was produced by the Au/Au_2O_3 oxidation at 1.36 volts. Since the solution was deoxygenated and under nitrogen, Au_2O (this species could be a chemisorbed layer of oxygen on the gold surface) must form through a mechanism such as is given in (1). If this is the case, the overall reaction occurring at 1.24 volts would be the production of oxygen through the following mechanism:

Reaction	Measured Potential
(1) $2Au + 3H_2O \rightleftarrows Au_2O_3 + 6H^+ + 6e^-$	1.36
(2) $Au_2O_3 \rightleftarrows Au_2O + O_2$	
(3) $Au_2O + 2H_2O \rightleftarrows Au_2O_3 + 4H^+ + 4e^-$	1.24
Sum of (2) and (3) $2H_2O \quad 4H^+ + O_2 + 4e^-$	1.24 v.

Additional evidence for this reaction is the formation of very small bubbles on the surface of the gold electrode during the long oxidation process at 1.24 volts.

Cathodic curves following anodic polarization to oxygen evaluation (Figure 14) show two electrochemical reductions occurring at 1.20 and 1.05 volts. According to the anodic reactions proposed, the potentials would correspond to the reductions of Au_2O_3/Au and at Au_2O_3/Au_2O, respectively. The number of coulombs necessary to effect the reductions varies somewhat with the time of previous anodic polarization. However, a maximum value of 600 uc for each reaction was observed. The number of gold atoms involved in the Au_2O_3/Au reaction would be about 1.2×10^{15} and in the Au_2O_3/Au_2O reaction 1.9×10^{15}. If the actual surface contained 3×10^{15} gold atoms as calculated, the entire surface would not participate in the reactions, but rather one would expect a patchwork of reaction sites.

Distortion of the linear double-layer charging curve in the potential region of ca 0.1 volt has been found previously by Hickling and has been attributed to the reduction of oxygen on the surface. According to the mechanism outlined above, the investigation must support this view in that some Au_2O is present before this potential is reached. El Wakkad and El Din found a distinct arrest at 0.4 volt on cathodic charging. The lone experiments where this behavior was found in the present system were when the electrolyte was deliberately saturated with oxygen. Under these conditions (Figure 16), a long reduction curve began at 0.4 volt and continued with a gradual decline in potential at low current densities (ca 0.2 ma/cm^2).

Cathodic decay curves show clearly that three separate electrochemical processes are occurring (Figure 15). Arrests at 1.36, 1.24, and 0.36 volt, respectively, correspond to Au_2O_3/Au, Au_2O_3/Au_2O and Au_2O/Au reactions.

Within the current density range of the investigation, the data do not substantiate the charging curve results of El Wakkad and El Din who found anodic arrests corresponding to the reactions Au/Au_2O and Au/AuO

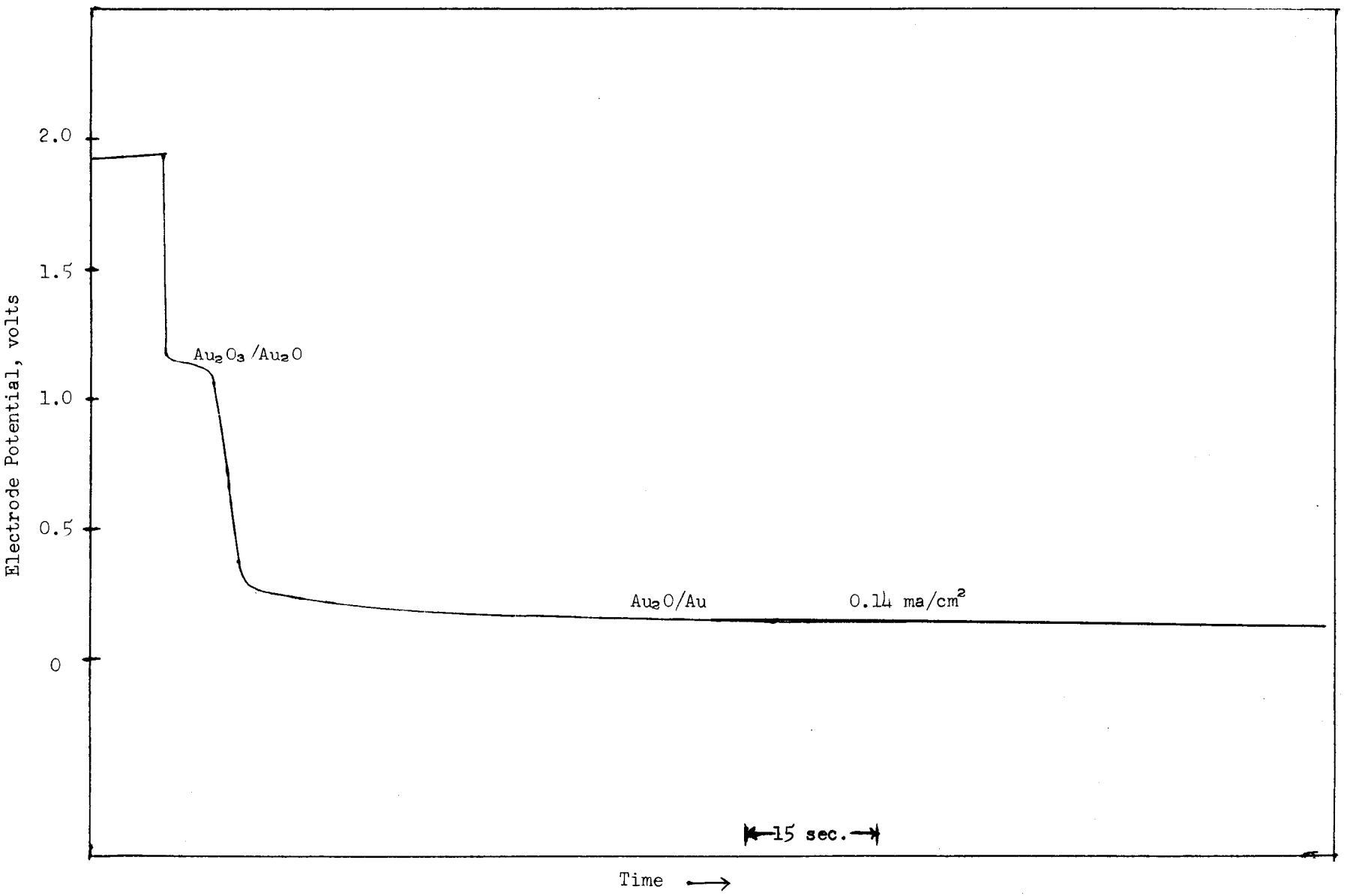
2.0
1.5
1.0
0.5
0
Electrode Potential, volts
Au2O3 /Au2O
Au2O/Au
0.14 ma/cm2
15 sec.
Time

Figure 16.

at 0.27 and 0.98 volt, respectively, in 0.1 H_2SO_4 electrolyte. At very low current densities (or 10 $\mu A/cm^2$), however, a slight distortion of the double-layer curve is observed in the region of these potentials. The rate of the reaction Au/Au_2O presumably is not sufficient to support the higher current densities, but the oxygen in the electrolyte reacts with the gold surface to form Au_2O once this potential region is passed. The Au_2O is then converted to Au_2O_3 at 1.24 volts.

FUTURE PROGRAM

In order to resolve some of the anomalies so far observed in this study, it is imperative that the measurements, which have up to now been performed on a fuel cell with a thin saturated asbestos membrane electrolyte, be repeated in a cell with circulating electrolyte thereby facilitating the introduction of a reference electrode to determine the extent of polarization phenomena at each electrode independently.

Since all of the work to date has been performed on co-catalyzed (platinum-palladium) Clevite porous nickel electrodes, it now becomes necessary to study the phenomena using alternate forms of electrode such as American Cyanamid teflon-paltinum-palladium black. In order to determine whether the primary effect is chemical or physical, electrodes with differing porosity should be investigated.

In the original disclosure to the Research and Technology Division, W-PAFB, Contract AF33(657)-7564, regarding improvements to fuel cell operation, two aspects other than the simple pulsing were discussed, one being the application of a reverse potential during the off cycle to accelerate depolarization of the electrode, and the second the use of what may be described as an ultrasonic pulse for a similar purpose. It is clear from recent work at Union Carbide that the former could be regarded as possessing considerable potentiality and might be anticipated as facilitating the increase in duty cycle in the pulsing process. It would be anticipated that both of these techniques would be applied to measurements made under pulsed conditions with a varying duty cycle.

REFERENCES

1. T. J. Gray, R. B. Rozelle, and M. L. Soeder, Nature, 202, 181 (1964).
2. A. Hickling, Trans. Faraday Soc., 41, 333 (1945).
3. A. Hickling and G. G. Vrjosek, Trans. Faraday Soc., 57, 123 (1961).
4. A. Hickling, Trans. Faraday Soc., 42, 518 (1946).
5. G. Armstrong, F. R. Himsworth, and J. A. V. Butler, Proc. Roy. Soc., 143A, 89 (1933).
6. S. E. S. El Wakkad and A. M. S. El Din, J. Chem. Soc., 3098 (1954).
7. D. O. Hayward and B. M. W. Trapnell, Chemisorption, Second Edition, Butterworths, Washington, 1964.
8. G. M. Schmid and N. Hackerman, J. Electrochem. Soc., 109, 243 (1962).

DISTRIBUTION LIST FOR FUEL CELL REPORTS - GRANT NsG-384

National Aeronautics and Space Administration
Washington, D. C. 20546
Attn: Miss Millie Ruda/AFSS-LD (3)
Walter C. Scott/RPP (1)
Ernst M. Cohn/RNW (1)
George F. Esenwein/MSA (1)
John L. Sloop/RP (1)
A. M. Andrus/FC (1)
Fred Schulman/RN (1)
Miss Winnie M. Morgan (25)

National Aeronautics and Space Administration
Goddard Space Flight Center
Greenbelt, Maryland
Attn: Thomas Hennigan (1)

National Aeronautics and Space Administration
Lewis Research Center
21000 Brookpark Road
Cleveland, Ohio 44135
Attn: B. Lubarsky Mail Stop 86-1 (1)
Martin J. Saari " " " (1)
Robert L. Cummings " " " (1)
Harvey J. Schwartz " " " (1)
William J. Nagle " " " (1)
N. D. Sanders " " 302-1 (1)
N. T. Musial " " 77-1 (1)

National Aeronautics and Space Administration
Marshall Space Flight Center
Huntsville, Alabama
Attn: Philip Youngblood (1)
Eugene Cagle (1)

National Aeronautics and Space Administration
Manned Space Craft Center
Houston, Texas 77001
Attn: William R. Dusenbury (1)
Systems Evaluation and Development Division
Rich Building, 6040 Telephone Road
Robert Cohen, Gemini Project Office

Jet Propulsion Laboratory
4800 Oak Grove Drive
Pasadena, California
Attn: Aiji Uchiyama (1)

DEPARTMENT OF THE ARMY

U. S. Army Engineer R and D Labs
Fort Belvoir, Virginia
Attn: Mr. B. C. Almaula (1)
Electrical Power Branch

U. S. Army Engineer R and D Labs
Fort Monmouth, New Jersey
Attn: David Linden (Code SELRA/SL-PS) (1)
Dr. Adelph Fischbach (Code SELRA/SL-PS) (1)
Arthur F. Daniel (Code SELRA/SL-PS) (1)

U. S. Army Research Office
Physical Sciences Division
3045 Columbia Pike
Arlington, Virginia
Attn: Dr. Sidney J. Magram (1)

Harry Diamond Labs
Room 300, Bldg. 92
Connecticut Avenue and Van Ness Street, N. W.
Washington, D. C.
Attn: Robert Goodrich (1)

U. S. Army Mobility Command
Research Division
Center Line, Michigan 48015
Attn: O. Renius (AMSMO-RR) (1)

U. S. Army Research Office
Box CM, Duke Station
Durham, North Carolina
Attn: Paul Greer (1)
Dr. Wilhelm Jorgensen (1)

Research Office
R and D Directorate
Army Weapons Command
Rock Island, Illinois 61201
Attn: G. Ransmith, Chief (1)

DEPARTMENT OF THE NAVY

Office of Naval Research
Department of the Navy
Washington, D. C. 20546
Attn: Dr. Ralph Roberts (1)
Dr. J. C. White (1)
H. W. Fox (Code 425) (1)

Bureau of Ships
Department of the Navy
Washington, D. C. 20546
Attn: Bernard B. Rosenbaum (Code 340) (1)
C. F. Viglotti (Code 660) (1)
James B. Trout (Code 660S) (1)
CDR Joseph W. Thornbury (Code 649) (1)

Naval Ordnance Laboratory
Department of the Navy
Corona, California
Attn: Mr. William C. Spindler (Code 441) (1)

Naval Ordnance Laboratory
Department of the Navy
Silver Spring, Maryland
Attn: Philip B. Cole (Code WB) (1)

DEPARTMENT OF THE AIR FORCE

Systems Engineering Group
RTD, AFSC, USAF
Wright-Patterson Air Force Base, Ohio 45433
Attn: George W. Sherman (1)
Robert L. Kerr (1)
James E. Cooper (1)
ASRCEM-1 (1)

AF Cambridge Research Lab
Attn: Crze (1)
L. G. Hanscom Field
Bedford, Massachusetts
Attn: Francis X. Doherty (1)
Edward Raskind (Wing F) (1)
Commander (CRO) (1)

Rome Air Development Center, ESD
Griffiss AFB, New York
Attn: Commander (RAALD) (1)
Frank J. Mollura (RASSM) (1)

Hq., USAF (AFRST-PM)
Washington, D. C. 20546
Attn: LT COL William G. Alexander (1)

CAPT William H. Ritchie (1)
Sapece Systems Division
Attn: SSZAE-11
Air Force Unit Post Office
Los Angeles, California 90045

CAPT William Hoover (1)
Air Force Ballistic Missile Division
Attn: WEZYA-21
Air Force Unit Post Office
Los Angeles, California 90045

ADVANCED RESEARCH PROJECTS AGENCY

Mr. Charles F. Yost (1)
Asst. Director, Material Sciences
Advanced Research Projects Agency
The Pentagon, Room 3E 153
Washington, D. C. 20546

Dr. John H. Huth (1)
Advanced Research Projects Agency
The Pentagon, Room 3E 157
Washington, D. C. 20546

ATOMIC ENERGY COMMISSION

U. S. Atomic Energy Commission (1)
Auxiliary Power Branch (SNAP)
Division of Reactor Development
Washington, D. C. 20546

LT COL John H. Anderson (1)
Advanced Space Reactor Branch
Division of Reactor Development
U. S. Atomic Energy Commission
Washington, D. C. 20546

OTHER GOVERNMENT AGENCIES

Defense Documentation Center Hq. (1)
Cameron Station, Bldg. 5
5010 Duke Street
Alexandria, Virginia 22314
Attn: TISIA

Office, DDR&E: USW & BSS
The Pentagon
Washington, D. C. 20546
Attn: G. B. Wareham (1)

Institute for Defense Analyses
R&D Support Division
1666 Connecticut Avenue, N. W.
Washington, D. C. 20549
Attn: Dr. George C. Szego (1)

Power Information Center (1)
University of Pennsylvania
Moore School Building
200 South 33rd Street
Philadelphia, Pennsylvania 19104

Office of Technical Services (1)
Department of Commerce
Washington, D. C. 20009

PRIVATE INDUSTRY

American Cyanamid Company
1937 W. Main Street
Stamford, Connecticut 06901
Attn: Dr. R. G. Haldeman (1)

Allis-Chalmers Mfg. Co.
110 S. 70th Street
Milwaukee, Wisconsin 53201
Attn: Dr. T. G. Kirkland (1)

Allison Division of General Motors
Indianapolis, Indiana 46206
Attn: Dr. Robert E. Henderson (1)

Astropower, Inc.
2968 Randolph Avenue
Costa Mesa, California 92629
Attn: Dr. Carl Berger (1)

Battelle Memorial Institute
Columbus, Ohio 43201
Attn: Dr. C. L. Faust (1)

Bell and Howell Research Center
360 Sierra Madre Villa
Pasadena, California
Attn: Alan G. Richards (1)

Bell Telephone Laboratories, Inc.
Murray Hill, New Jersey 07971
Attn: Mr. U. B. Thomas (1)

Electrochemica Corp.
1140 O'Brien Drive
Menlo Park, California 94025
Attn: Dr. Morris Eisenberg (1)

Electro-Optical Systems, Inc.
300 North Halstead Street
Pasadena, California
Attn: Dr. Joseph Neustein (1)

Engelhard Industries, Inc.
497 Delancy Street
Newark, New Jersey 07105
Attn: Dr. J. G. Cohn (1)

ESSO Research and Engineering Company
Products Research Division
P. O. Box 215
Linden, New Jersey 07036
Attn: Dr. Carl Heath (1)

Ford Motor Company
Aeronutronics Division
Newport Beach, California
Attn: Dr. R. C. Bean (1)

General Electric Company
Direct Energy Conversion Operations
Lynn, Massachusetts
Attn: Dr. E. Oster (1)

General Electric Company
Research Laboratory
Schenectady, New York
Attn: Dr. H. Liebhafsky (1)

General Electric Company
Missile & Space Vehicle Dept.
P. O. Box 8555
Philadelphia, Pennsylvania 19101
Attn: A. D. Taylor (1)

Globe-Union, Inc.
900 East Keefe Avenue
Milwaukee, Wisconsin 53201
Attn: Dr. C. K. Morehouse (1)

Hoffman Electronics Company
Research Laboratory
Santa Barbara, California
Attn: Dr. Joseph Smatko (1)

Johns Hopkins University
Applied Physics Laboratory
8621 Georgia Avenue
Silver Spring, Maryland
Attn: W. A. Tynan (1)

Leesona-Moss Laboratories
Lake Success Park
Community Drive
Great Neck, New York
Attn: Dr. A. Moos (1)

Lockheed Missiles & Space Company
Sunnyvale, California 94086
Attn: Dr. George B. Adams (1)

Livingston Electronic Corporation
Route 309
Montgomeryville, Pennsylvania 18936
Attn: William F. Myers (1)

McDonnell Aircraft Corporation
Attn: Project Gemini Office (1)
P. O. Box 516
St. Louis, Missouri 63166

Monsanto Research Corporation
Everett, Massachusetts
Attn: Dr. J. O. Smith (1)

North American Aviation Company
S&ID Division
Downey, California
Attn: Dr. James Nash (1)

Pratt & Whitney Aircraft Division
United Aircraft Corporation
East Hartford, Connecticut 06108
Attn: Librarian (1)

Radio Corporation of America
Astro Division
Heightstown, New Jersey
Attn: Dr. Seymour Winkler (1)

Radio Corporation of America
Somerville, New Jersey 08876
Attn: Dr. G. Lozier (1)

Thompson Ramo Wooldridge Inc.
23555 Euclid Avenue
Cleveland, Ohio 44117
Attn: Librarian (1)

Union Carbide Corporation
12900 Snow Road
Parma, Ohio
Attn: Dr. George E. Evans (1)

University of California
Space Science Laboratory
Berkeley, California 94704
Attn: Prof. Charles W. Tobias (1)

University of Pennsylvania
Electrochemistry Laboratory
Philadelphia, Pennsylvania 19104
Attn: Prof. John O.'M. Bockris (1)

Western Reserve University
Cleveland, Ohio
Attn: Prof. Ernest Yeager (1)

Yardney Electric Corporation
New York, New York
Attn: Dr. Paul Howard (1)

NASA, Ames Research Center
Pioneer Project
Moffett Field, California 94035
Attn: James R. Swain (1)